What is Digital Holographic Microscopy (DHM)? What is the state of the art? How can DHM be applied to Marine Environment research?

Ana Doblas

Department of Electrical & Computer Eng.

The University of Memphis, USA

Research Symposium, PD Spain – Memphis Program

Thursday, July 13th, 2023

Optical Imaging Research Lab

Driven by doing.

THE UNIVERSITY OF MEMPHIS

Biological samples have poor contrast under bright-field microscopy

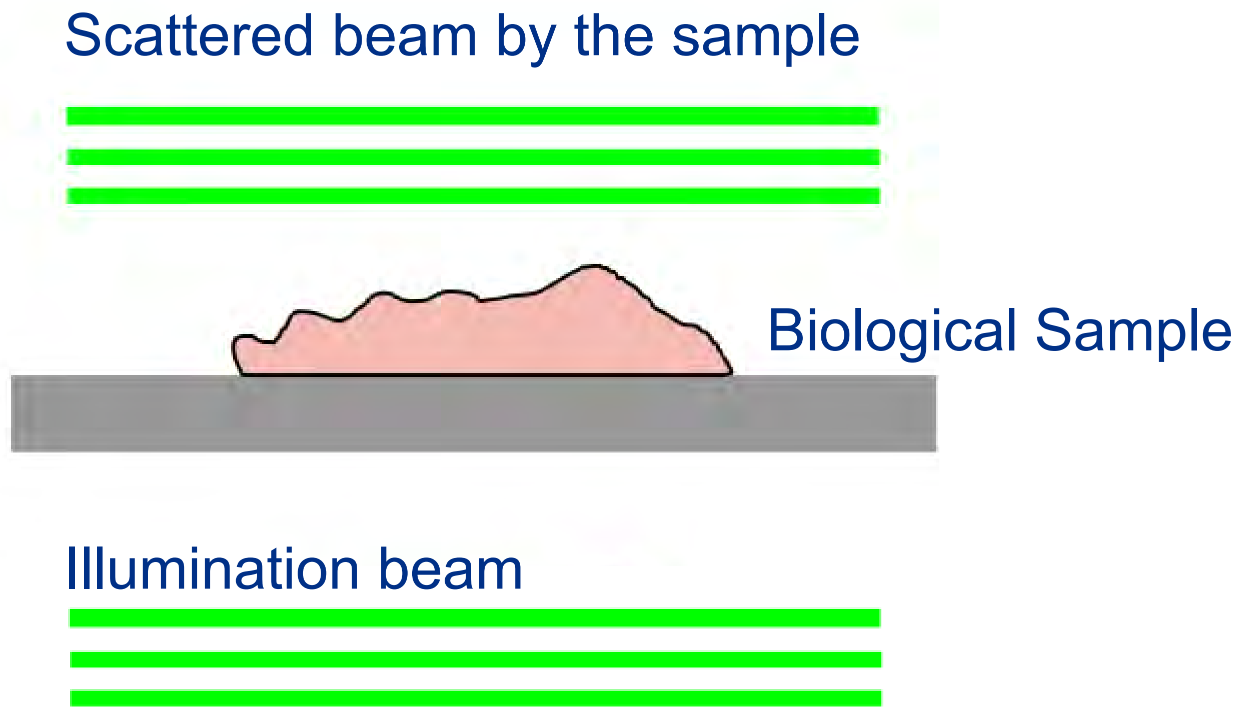

Unfixed, **unstained** human epithelial cells

Phase Imaging Techniques record phase changes into intensity images

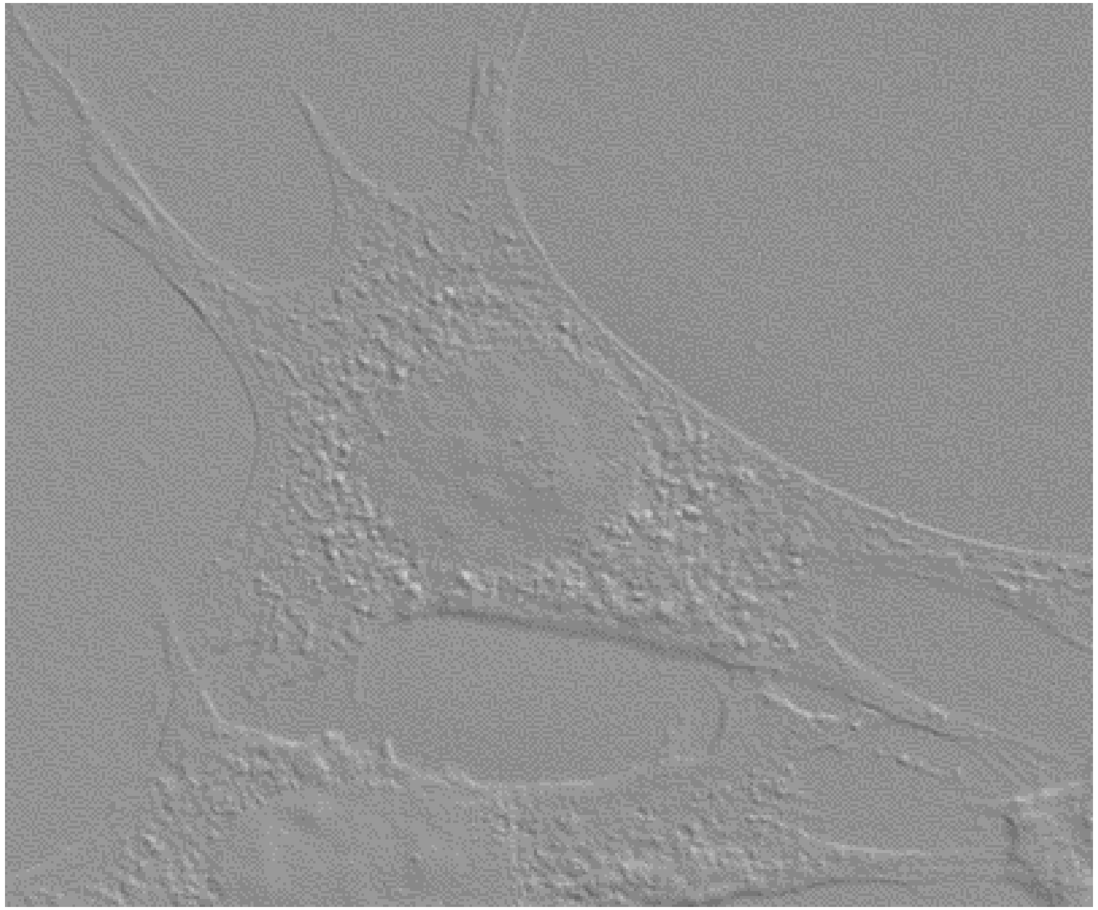

Principle of Quantitative Phase Imaging (QPI)

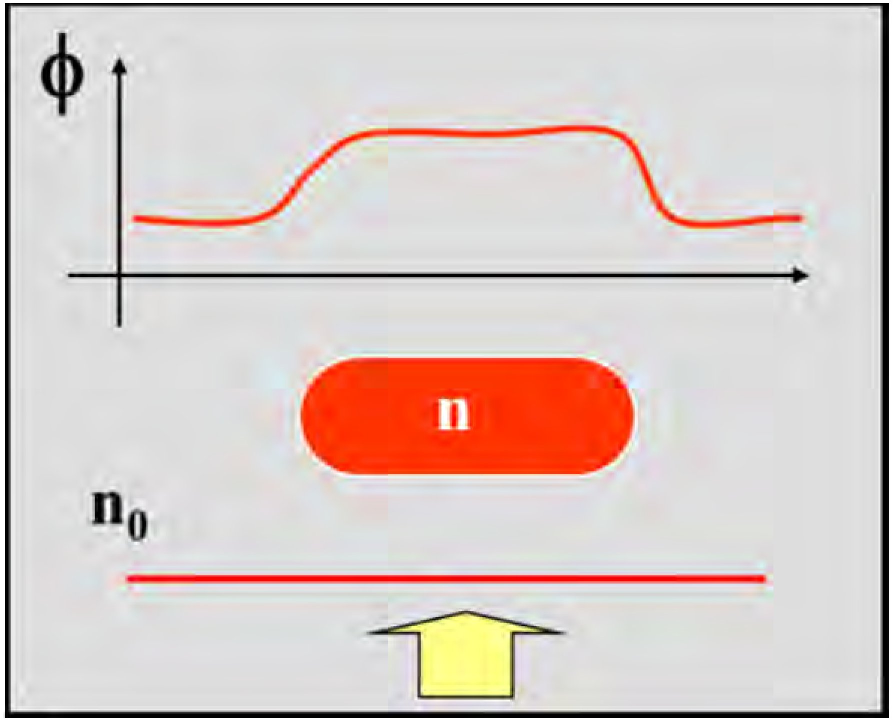

$$\phi = \frac{2\pi}{\lambda}(n - n_0)t$$

$$\text{known } (n, n_0) \rightarrow t,\ \text{topography}$$

$$\text{known } (t) \rightarrow (n - n_0),\ \text{refractometry}$$

Phase Images of human U87 glioblastoma cells

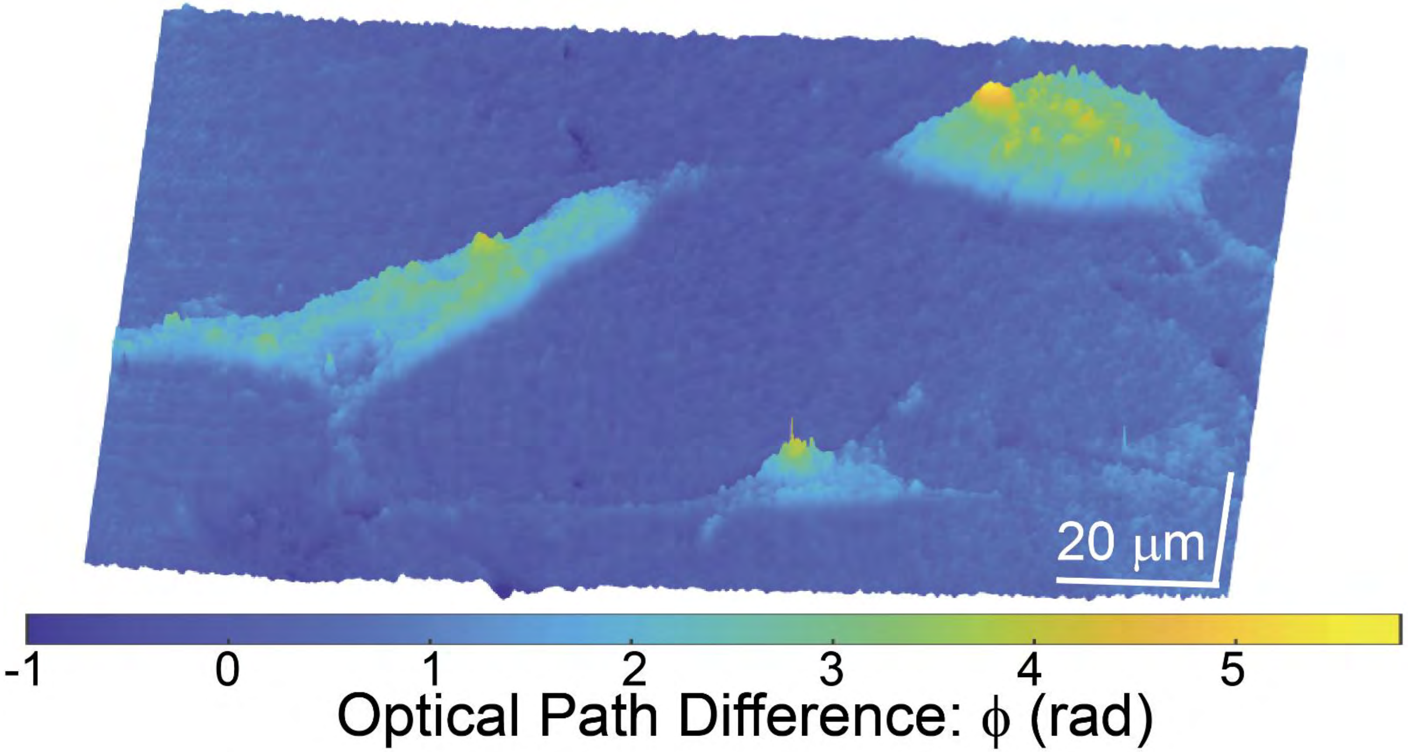

Digital Holographic Microscopy (DHM)

Highlights:

- **Label-free** (i.e., unstained) imaging technique.
- Digital Holographic Microscopy (DHM) permits the **reconstruction of the complex** (i.e., amplitude and phase) **wavefront** diffracted by a given specimen.
- By means of the acquisition of the complex information, one can **numerically refocus any axial plane** of the sample (i.e., particle-tracking applications).
- **Off-axis DHM** systems are suitable for **live imaging** since there are a **single-shot** method.

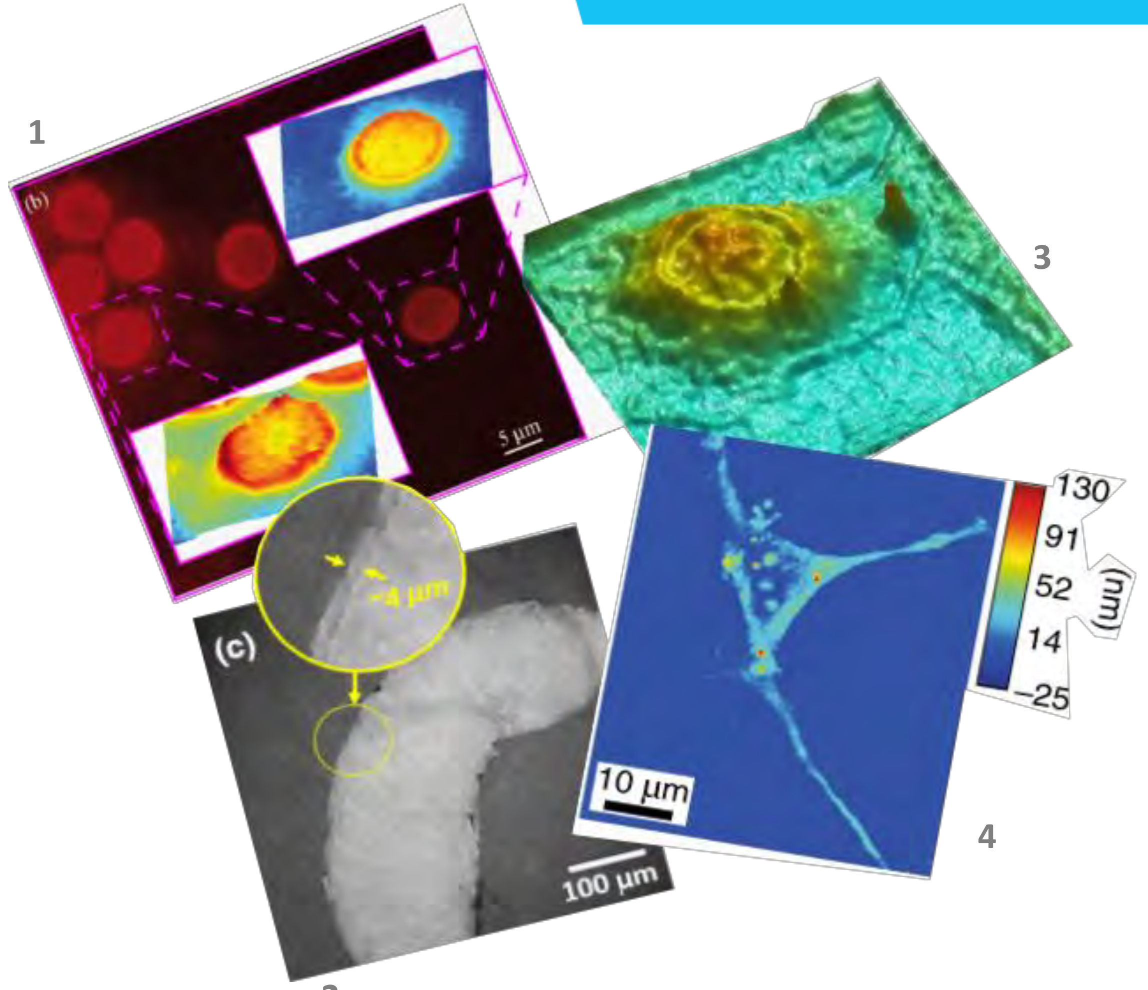

1. A. Doblas, *et. al.*, J. Biomed. Opt. 19, 46022 (2014).
2. C. Trujillo, *et. al.,* Appl. Opt. 55, 10299–10306 (2016).
3. M. K. Kim., J. Opt. Soc. Korea 14, 77–89 (2010).
4. Y. K. Park , *et. Al.*, Nat. Photonics 12, 578–589 (2018).

Applications of QPI-DHM in Life and Material Science

Some Applications of QPI

- ❑ Live-Cell Imaging
- ❑ Cell and Tissue Analysis
- ❑ Disease Diagnosis
- ❑ Disease Screening
- ❑ Cancer Pathology
- ❑ Drug Discovery

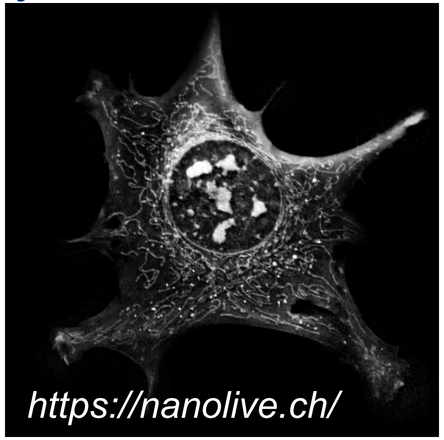

Some Applications in Material Science

- ❑ Dynamic Topography
- ❑ Defect Inspection
- ❑ Roughness Quality Control
- ❑ Surface Characterization
- ❑ Surface Analysis
  - ❑ Forensic Document Examination

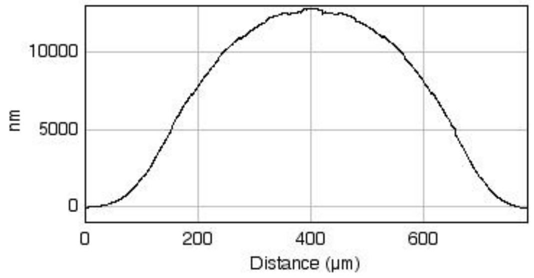

QPI: Quantitative Phase Imaging

Optical Recording Stage in DHM is the optical recording of an interference

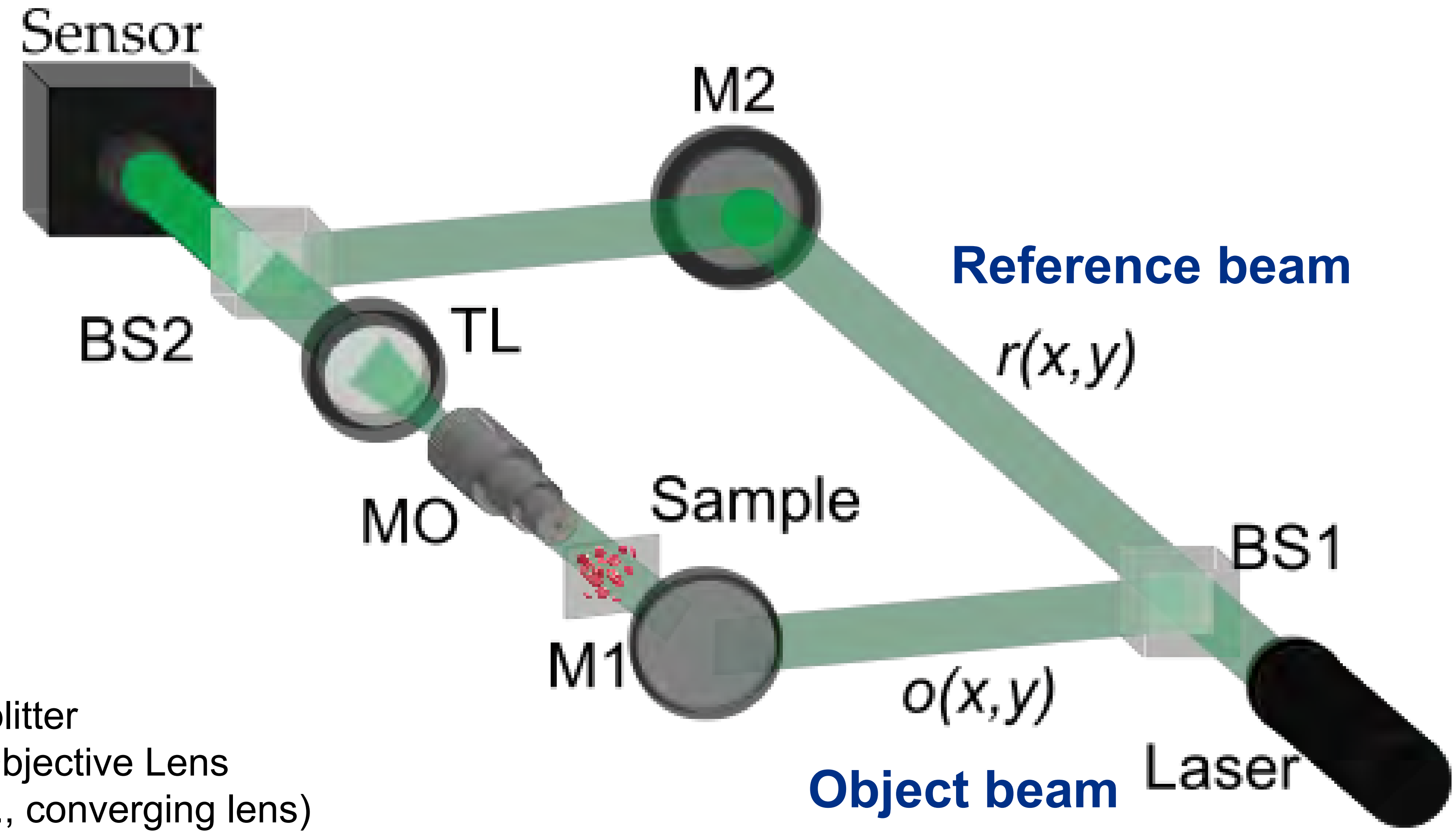

M1/M2: Mirrors
BS1/BS2: Beamsplitter
MO: Microscope Objective Lens
TL: Tube lens (e.g., converging lens)

Optical Recording Stage in DHM is the optical recording of an interference

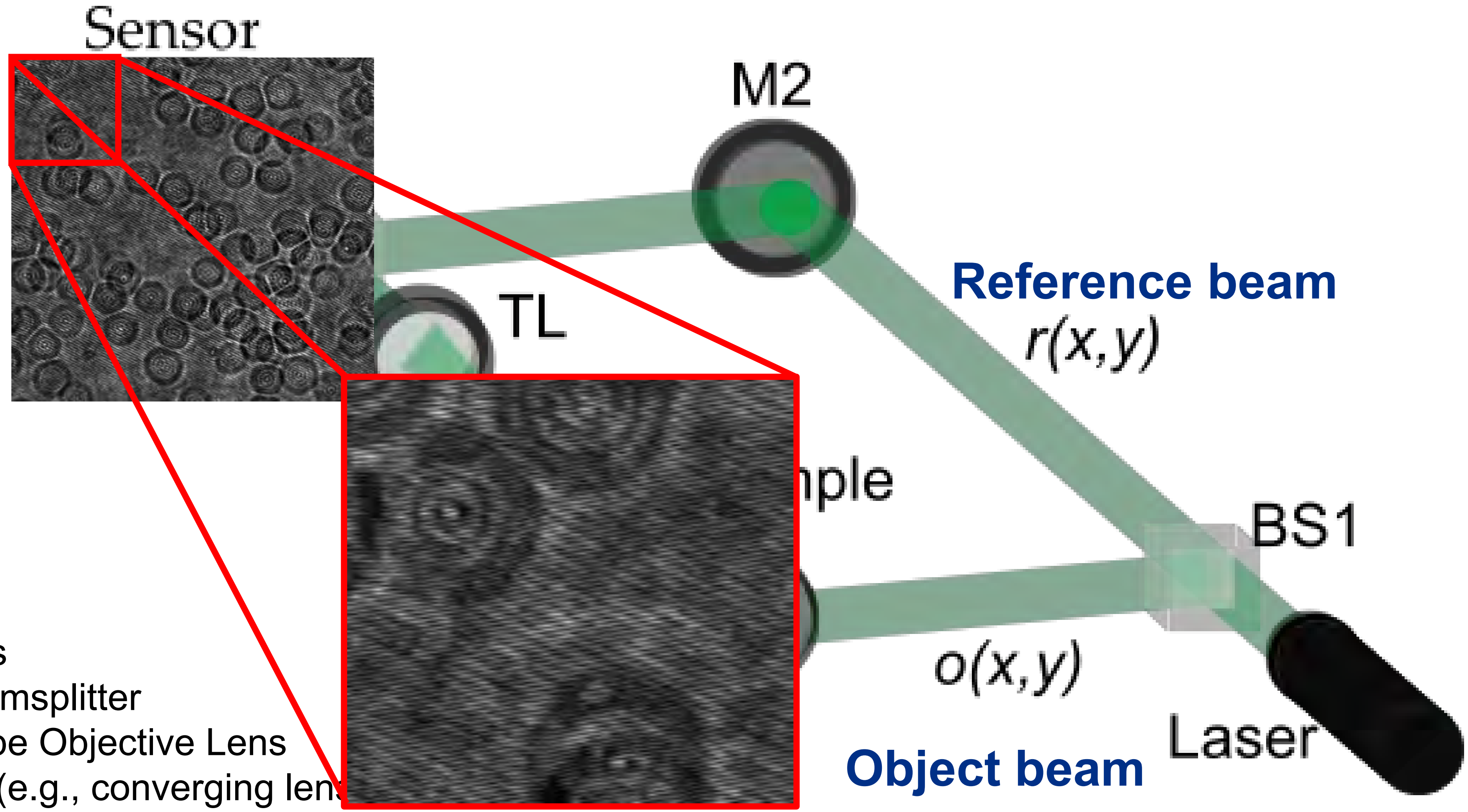

M1/M2: Mirrors
BS1/BS2: Beamsplitter
MO: Microscope Objective Lens
TL: Tube lens (e.g., converging len

Relation between Spatial and Fourier (frequency) Domain

Object
$o_{\mathrm{F}}(\boldsymbol{x})$

Object spectrum
$O_{\mathrm{F}}(\boldsymbol{u})$

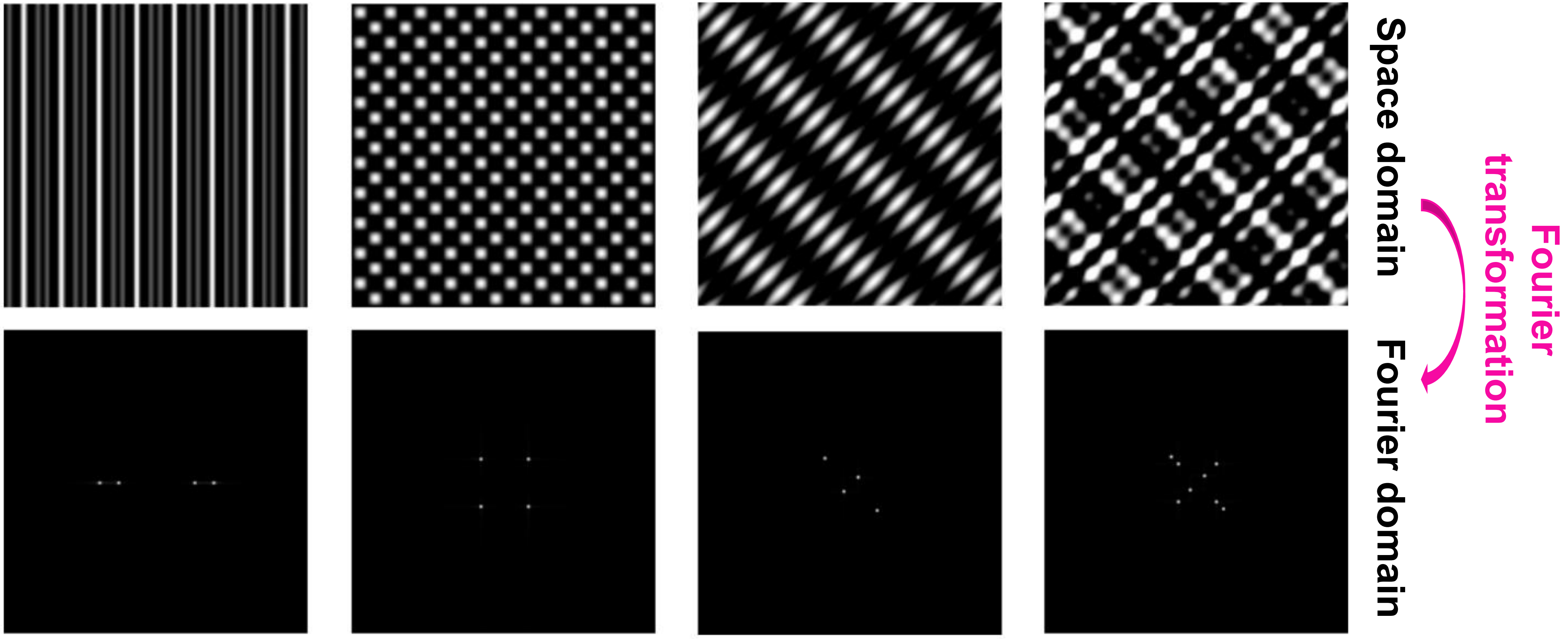

https://clearlyconfusedcarlo.wordpress.com/2016/09/29/activity-6-properties-and-applications-of-the-2d-fourier-transform/

Relation between Spatial and Fourier (frequency) Domain

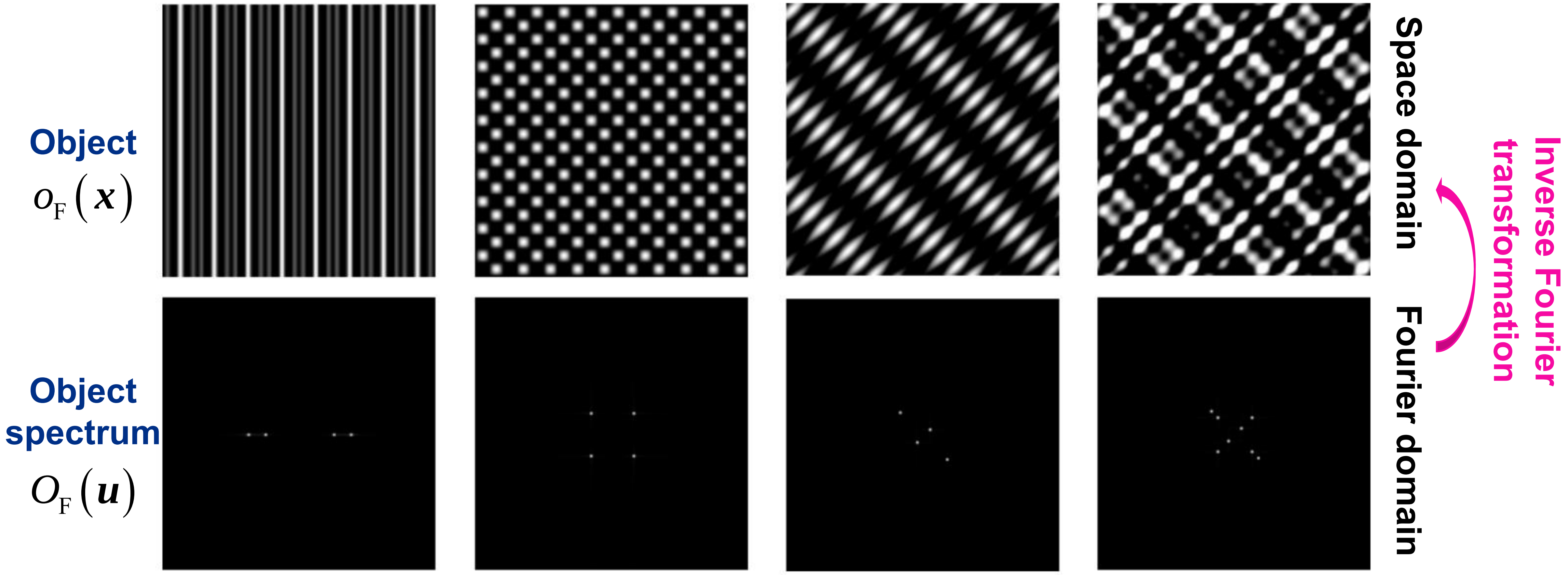

https://clearlyconfusedcarlo.wordpress.com/2016/09/29/activity-6-properties-and-applications-of-the-2d-fourier-transform/

Need of a numerical reconstruction method to decouple the complex information of the object

? = Information that we want to know

Hologram:

$$h(\mathbf{x}) = |u_{IP}(\mathbf{x})|^2 + |r(\mathbf{x})|^2 + u_{IP}(\mathbf{x})r^*(\mathbf{x}) + u_{IP}^*(\mathbf{x})r(\mathbf{x})$$

FT = Fourier Transform

?

FT Hologram:

$$H(\mathbf{u}) = DC(\mathbf{u}) + U(\mathbf{u}) \otimes_2 \delta(\mathbf{u} - \mathbf{k}) + U^*(\mathbf{u}) \otimes_2 \delta(\mathbf{u} + \mathbf{k})$$

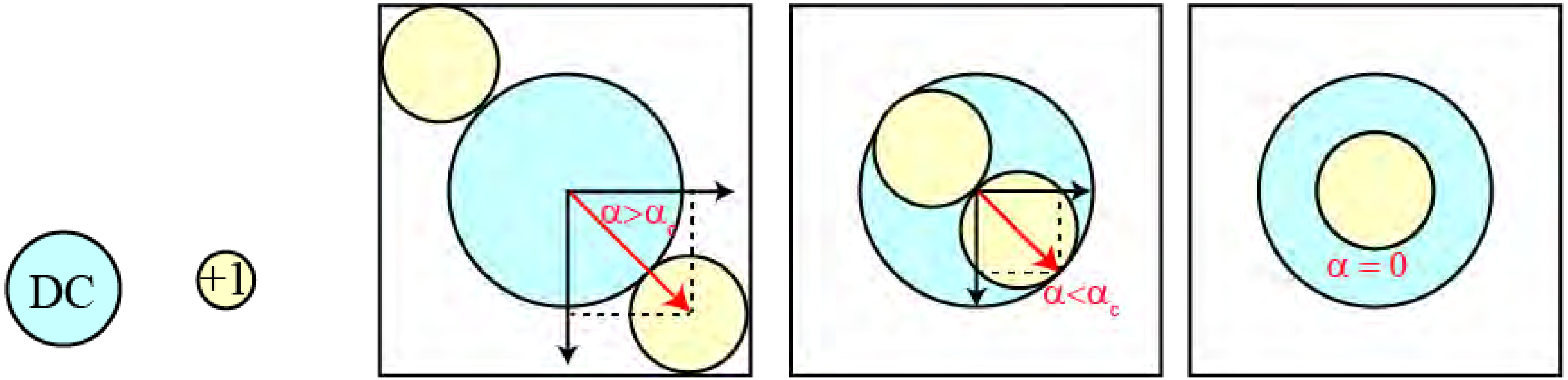

Off-axis | **Slightly off-axis** | **Strict in-line**

THE UNIVERSITY OF MEMPHIS

Application of spatial filtering in off-axis DHM systems

FT Hologram:

$$H(\mathbf{u}) = DC(\mathbf{u}) + U(\mathbf{u}) \otimes_2 \delta(\mathbf{u}-\mathbf{k}) + U^*(\mathbf{u}) \otimes_2 \delta(\mathbf{u}+\mathbf{k})$$

Off-axis DHM: Numerical Reconstruction

FT Hologram: $H(\mathbf{u}) = DC(\mathbf{u}) + U(\mathbf{u}) \otimes_2 \delta(\mathbf{u}-\mathbf{k}) + U^*(\mathbf{u}) \otimes_2 \delta(\mathbf{u}+\mathbf{k})$

Spatial Filtering

$$H_F(\mathbf{u}) = U_{IP}(\mathbf{u}) \otimes_2 \delta(\mathbf{u}-\mathbf{k})$$

Off-axis DHM: Numerical Reconstruction

FT Hologram: $H(\mathbf{u}) = DC(\mathbf{u}) + U(\mathbf{u}) \otimes_2 \delta(\mathbf{u}-\mathbf{k}) + U^*(\mathbf{u}) \otimes_2 \delta(\mathbf{u}+\mathbf{k})$

Spatial Filtering

$H_F(\mathbf{u}) = U_{IP}(\mathbf{u}) \otimes_2 \delta(\mathbf{u}-\mathbf{k})$

Ref. Compensation

$H(\mathbf{u}) \otimes_2 R(\mathbf{u}) = U_{IP}(\mathbf{u})$

Off-axis DHM: Numerical Reconstruction

FT Hologram: $H(\mathbf{u}) = DC(\mathbf{u}) + U(\mathbf{u}) \otimes_2 \delta(\mathbf{u}-\mathbf{k}) + U^*(\mathbf{u}) \otimes_2 \delta(\mathbf{u}+\mathbf{k})$

Spatial Filtering

$H_F(\mathbf{u}) = U_{IP}(\mathbf{u}) \otimes_2 \delta(\mathbf{u}-\mathbf{k})$

Ref. Compensation

$H(\mathbf{u}) \otimes_2 R(\mathbf{u}) = U_{IP}(\mathbf{u})$

FT^{-1}

$u_{IP}(\mathbf{x})$

Amplitude-contrast

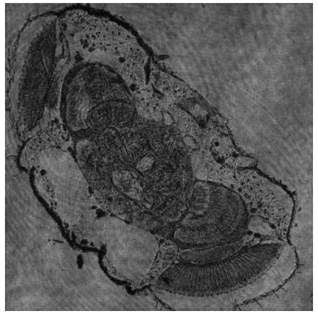

$a(\mathbf{x}) = \sqrt{|u_{IP}(\mathbf{x})|^2}$

Phase-contrast

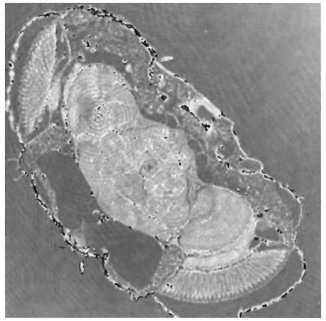

$\varphi(\mathbf{x}) = \text{atan}\left[\frac{\text{Im}(u_{IP})}{\text{Re}(u_{IP})}\right]$

THE UNIVERSITY OF MEMPHIS

The optical configuration of the DHM systems distorts the measurements of the reconstructed phase images

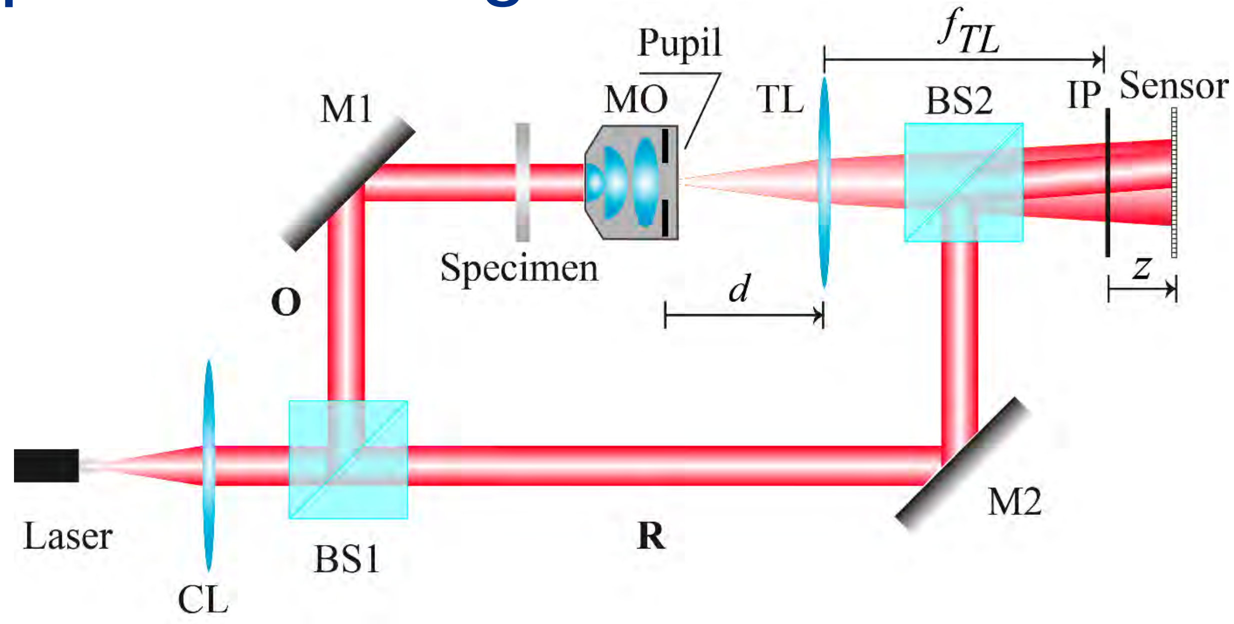

Complex amplitude distribution at the recording plane

$$u(\boldsymbol{x};z)=\frac{\mathrm{i}}{\lambda z}\mathrm{e}^{\mathrm{i}kz}\left\{u_{IP}(\boldsymbol{x})\otimes_2\exp\left(\mathrm{i}\frac{k}{2z}|\boldsymbol{x}|^2\right)\right\}$$

The optical configuration of the DHM systems distorts the measurements of the reconstructed phase images

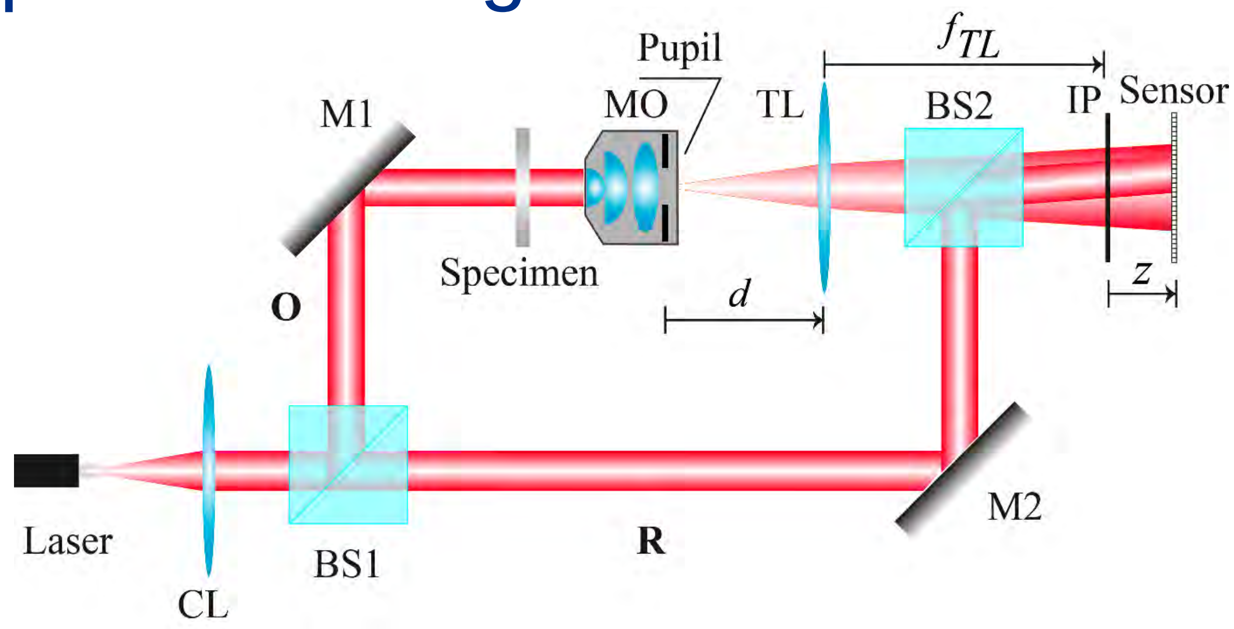

Complex amplitude distribution at the recording plane

$$u(\mathbf{x};z)=\frac{\mathrm{i}}{\lambda z}e^{\mathrm{i}kz}\left\{u_{IP}(\mathbf{x})\otimes_2\exp\left(\mathrm{i}\frac{k}{2z}|\mathbf{x}|^2\right)\right\}$$

Complex amplitude distribution at the image plane (IP)

$$u_{IP}(\mathbf{x})\propto\frac{1}{M^2}\exp\left(\mathrm{i}\frac{k}{2C}|\mathbf{x}|^2\right)\times\left\{o\left(\frac{\mathbf{x}}{M}\right)\otimes_2 P\left(\frac{\mathbf{x}}{\lambda f_{TL}}\right)\right\}$$

$$M=-f_{TL}/f_{MO}$$

$$C=f_{TL}^2/(f_{TL}-d)$$

THE UNIVERSITY OF MEMPHIS

Doblas *et al.*, *Opt. Letters* 38, 1352 (2013).

Non-telecentric DHM systems are shift-variant imaging systems

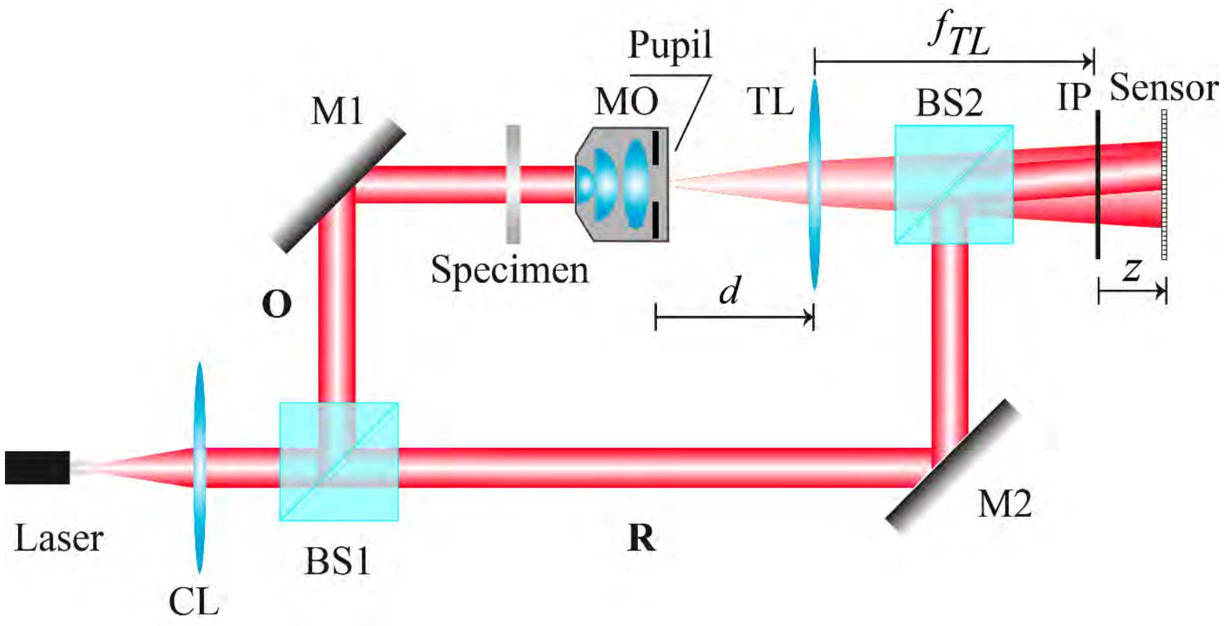

Complex amplitude distribution at the recording plane

$$u(\mathbf{x};z)=\frac{\mathrm{i}}{\lambda z}e^{\mathrm{i}kz}\left\{u_{IP}(\mathbf{x})\otimes_2 \exp\left(\mathrm{i}\frac{k}{2z}|\mathbf{x}|^2\right)\right\}$$

Complex amplitude distribution at the image plane (IP)

$$u_{IP}(\mathbf{x})\propto\frac{1}{M^2}\exp\left(\mathrm{i}\frac{k}{2C}|\mathbf{x}|^2\right)\times\left\{o\left(\frac{\mathbf{x}}{M}\right)\otimes_2 P\left(\frac{\mathbf{x}}{\lambda f_{TL}}\right)\right\}$$

$$M=-f_{TL}/f_{MO}$$

$$C=f_{TL}^2/\left(f_{TL}-d\right)$$

Non-Telecentric DHM

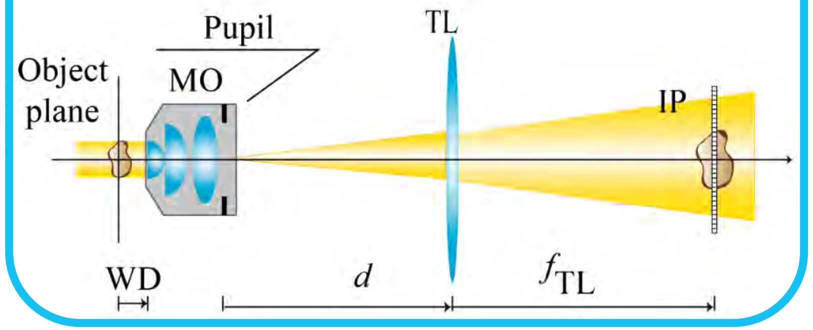

Doblas *et al.*, *Opt. Letters* 38, 1352 (2013).

Accurate Quantitative Phase Imaging by DHM systems operating in the telecentric regime

$M = -f_{TL} / f_{MO}$

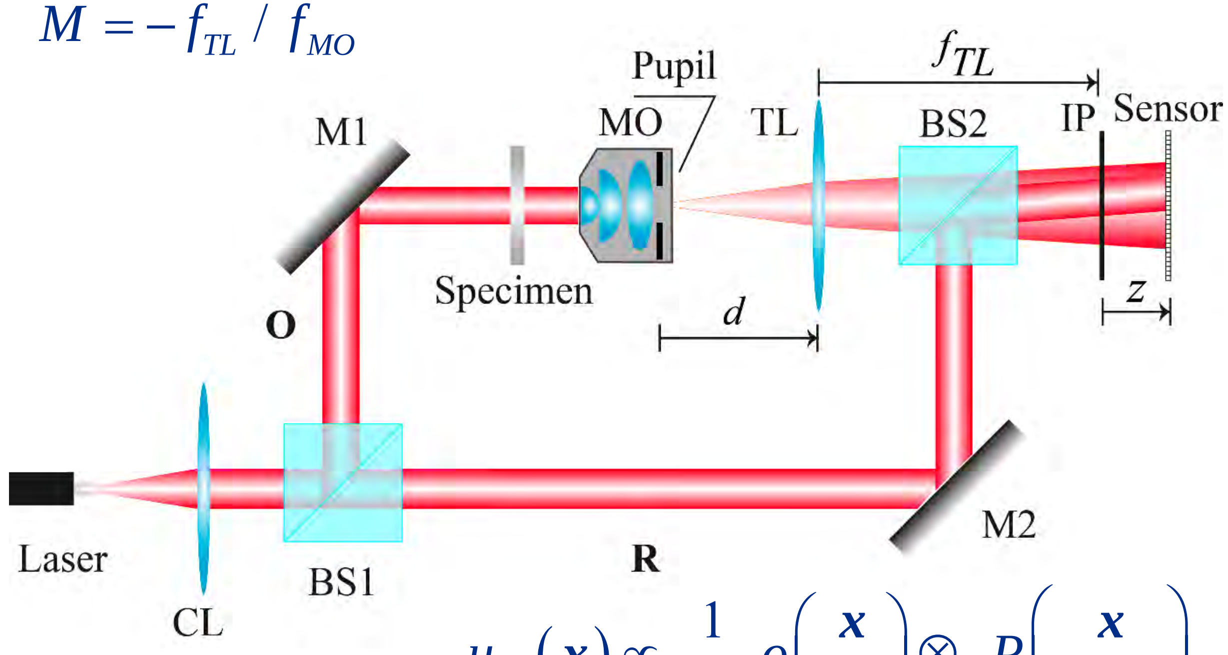

$$u_{IP}(\mathbf{x}) \propto \frac{1}{M^2} o\left(\frac{\mathbf{x}}{M}\right) \otimes_2 P\left(\frac{\mathbf{x}}{\lambda f_{TL}}\right)$$

Complex amplitude distribution at the recording plane

$$u(\mathbf{x};z) = \frac{\mathrm{i}}{\lambda z} \mathrm{e}^{\mathrm{i}kz} \left\{ u_{IP}(\mathbf{x}) \otimes_2 \exp\left(\mathrm{i}\frac{k}{2z}|\mathbf{x}|^2 \right) \right\}$$

Complex amplitude distribution at the image plane (IP)

$$u_{IP}(\mathbf{x}) \propto \frac{1}{M^2} \exp\left(\mathrm{i}\frac{k}{2C}|\mathbf{x}|^2 \right) \times \left\{ o\left(\frac{\mathbf{x}}{M}\right) \otimes_2 P\left(\frac{\mathbf{x}}{\lambda f_{TL}}\right) \right\}$$

Telecentric DHM

$d = f_{TL}; C = \infty$

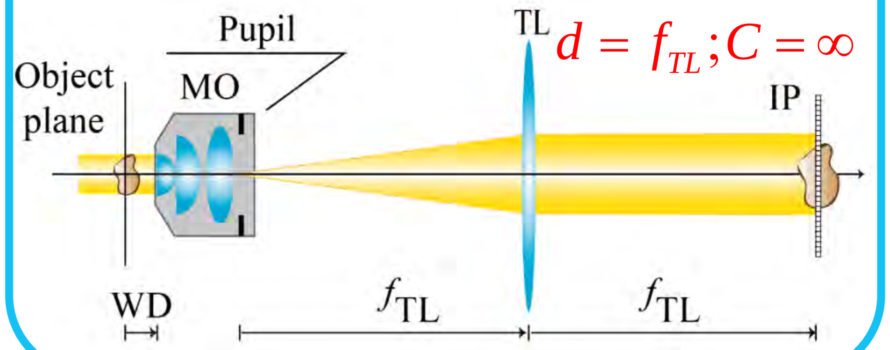

Doblas *et al.*, *Opt. Letters* 38, 1352 (2013).

Accurate Quantitative Phase Imaging by DHM systems operating in the telecentric regime

$$M = -f_{TL} / f_{MO}$$

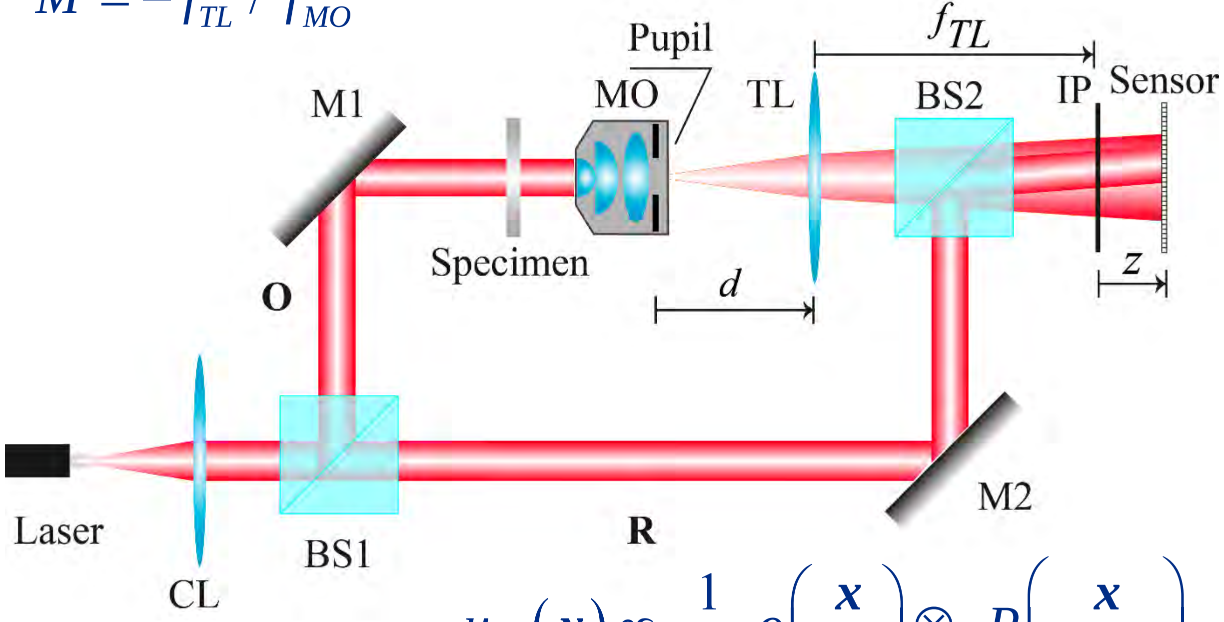

$$u_{IP}(\mathbf{x}) \propto \frac{1}{M^2} o\left(\frac{\mathbf{x}}{M}\right) \otimes_2 P\left(\frac{\mathbf{x}}{\lambda f_{TL}}\right)$$

Complex amplitude distribution at the recording plane

$$u(\mathbf{x};z) = \frac{\mathrm{i}}{\lambda z} e^{\mathrm{i}kz} \left\{ u_{IP}(\mathbf{x}) \otimes_2 \exp\left(\mathrm{i}\frac{k}{2z}|\mathbf{x}|^2\right) \right\}$$

Complex amplitude distribution at the image plane (IP)

$$u_{IP}(\mathbf{x}) \propto \frac{1}{M^2} \exp\left(\mathrm{i}\frac{k}{2C}|\mathbf{x}|^2\right) \times \left\{ o\left(\frac{\mathbf{x}}{M}\right) \otimes_2 P\left(\frac{\mathbf{x}}{\lambda f_{TL}}\right) \right\}$$

Telecentric DHM

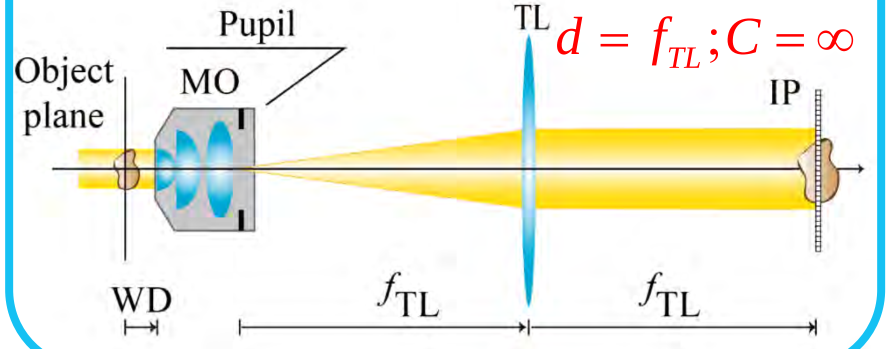

$$d = f_{TL}; C = \infty$$

<u>SHIFT-INVARIANT</u> IMAGING TECHNIQUE FOR <u>TELECENTRIC-BASED</u> DHM

Doblas *et al.*, *Opt. Letters* 38, 1352 (2013).

Advantages of telecentric-cased DHM systems

The imaging system is **shift-invariant**.

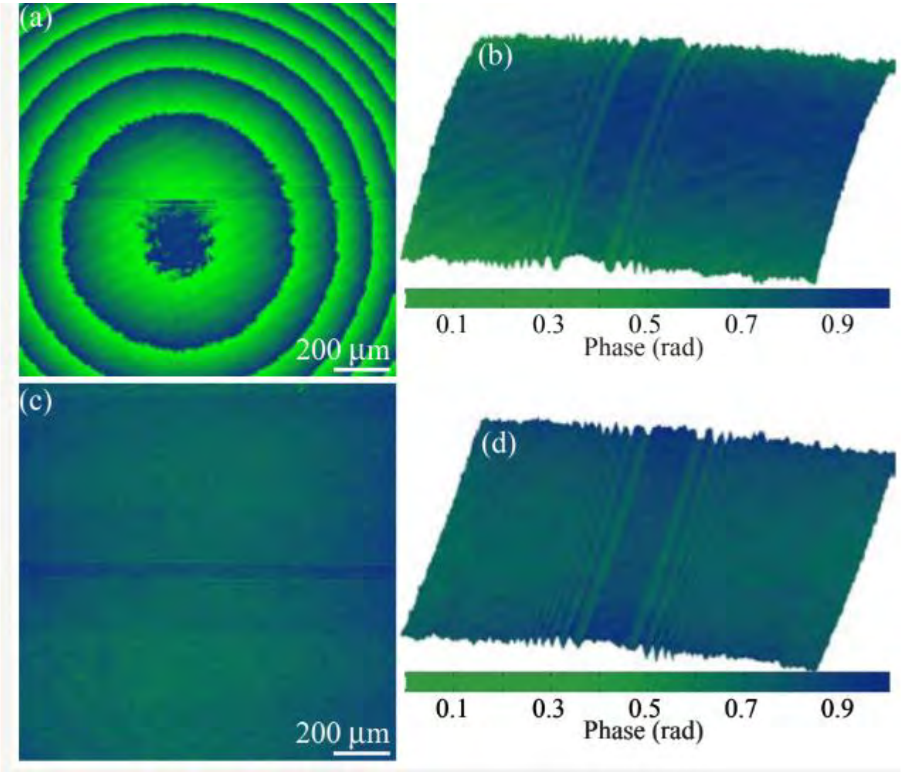

Doblas *et al.*, *Opt. Letters* 38, 1352 (2013).
Doblas *et al.*, *J. Biomed. Opt. 19*, 046022 (2014).

Advantages of telecentric-cased DHM systems

The imaging system is **shift-invariant**.

Preservation of the accuracy of the **quantitative phase measurement** over the whole field of view.

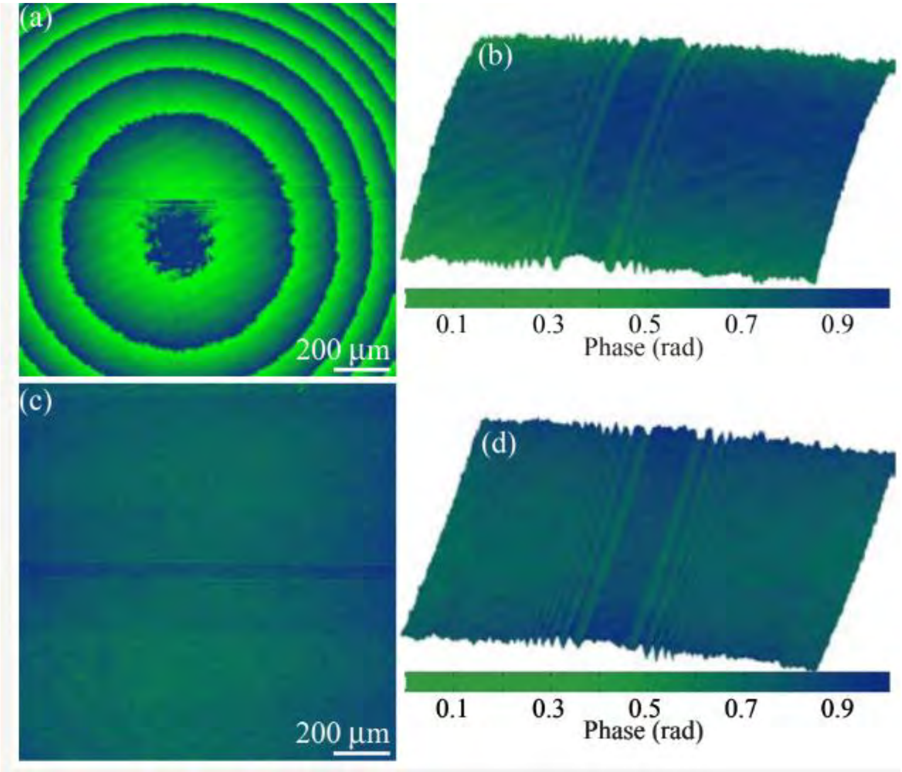

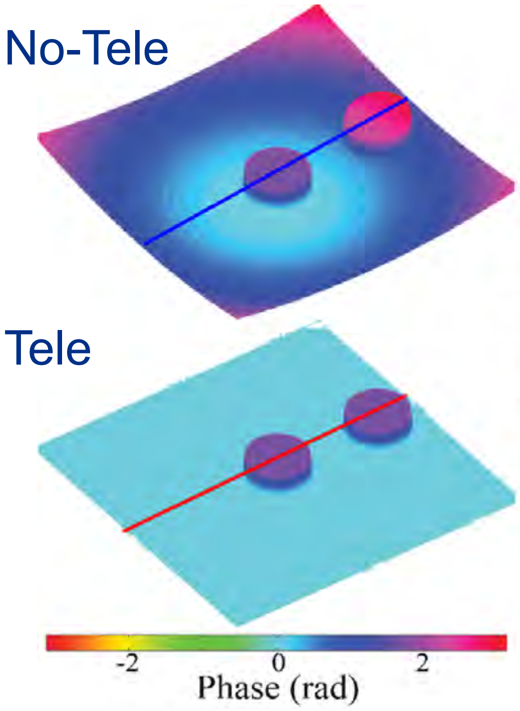

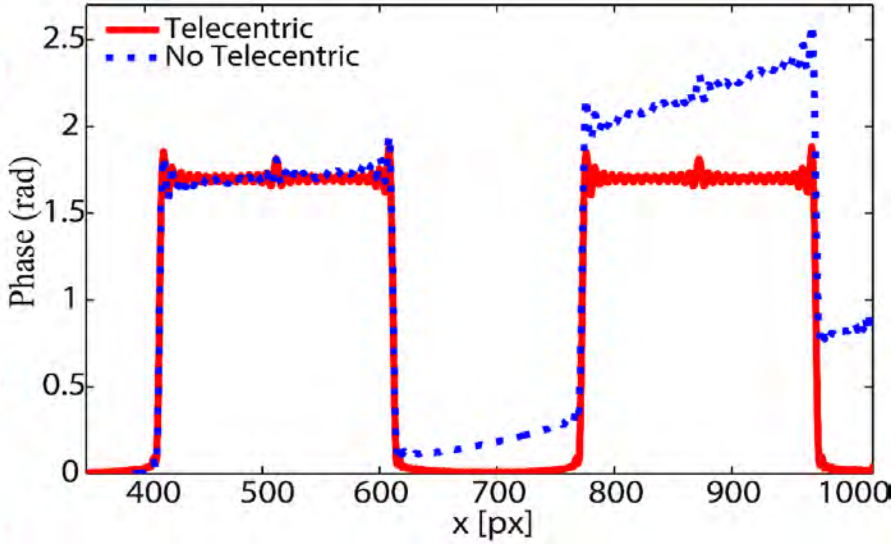

THE UNIVERSITY OF MEMPHIS

Doblas *et al.*, *Opt. Letters* 38, 1352 (2013).
Doblas *et al.*, *J. Biomed. Opt. 19*, 046022 (2014).

Advantages of telecentric-based DHM systems

Preservation of the **resolution limit** imposed by the numerical aperture of the objective lens

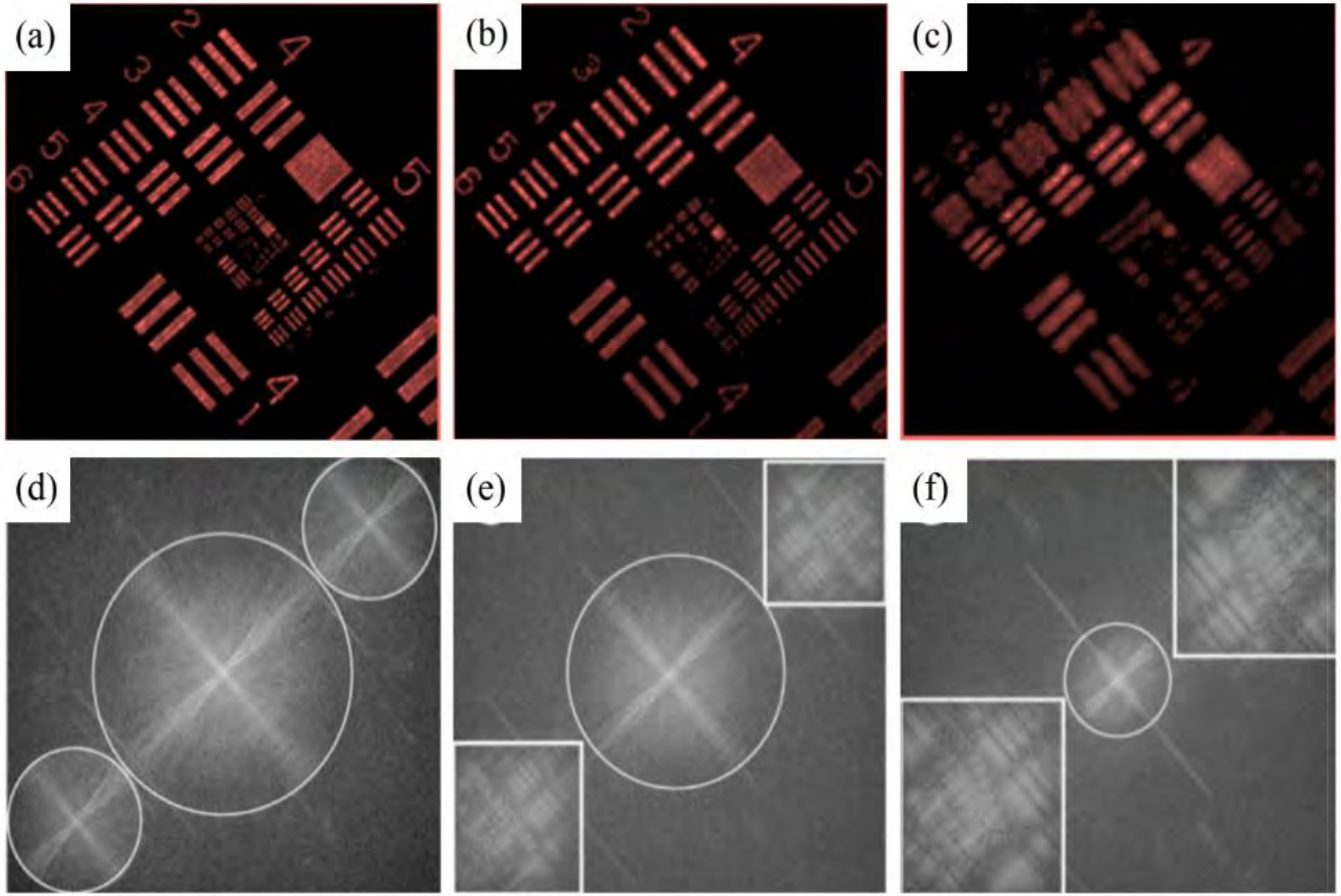

Sanchez-Ortiga & Doblas *et al.*, Appl. Opt. 53, 2058 (2013).

Telecentric-based DHM as a screening technology for Diabetes

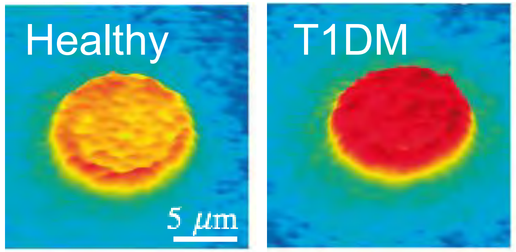

- ☑ Pilot study (43 participants) to demonstrate **telecentric-DHM** as a **tool** of **diagnosing diabetes**.
- ☑ Our experimental results indicate **two distinctive groups** of phase values.
- ☑ **Phase value above 3.40 rad** are an indication of hyperglycemia, being like Hb1AC values above 6.5 % which are diagnostic of diabetes.

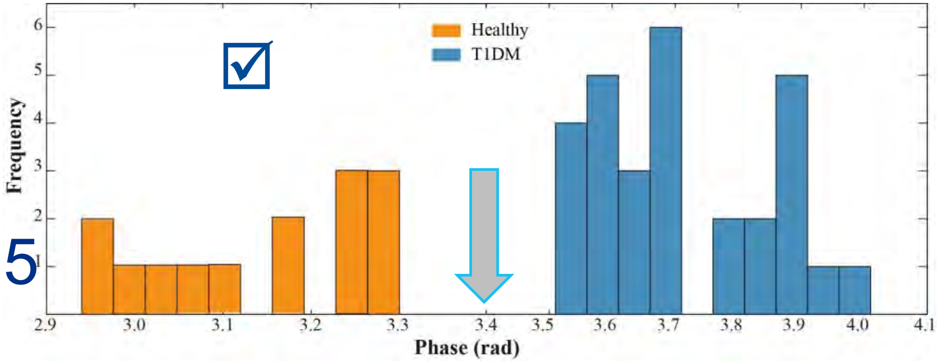

- ☑ From the strong correlation between the Hb1AC and phase values, we conclude that the phase measurement may provide an index of average blood glucose over a long period of time.

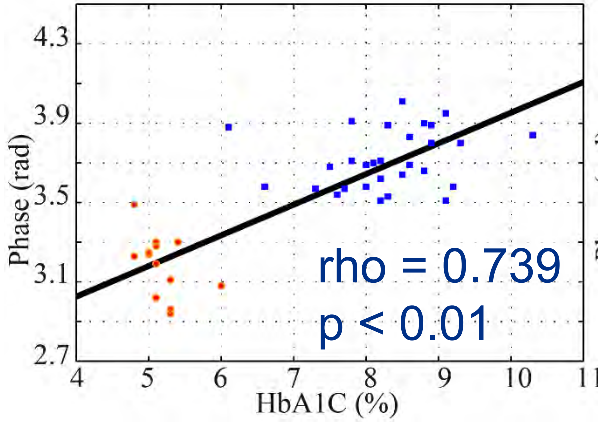

Doblas *et al.*, *J. Microsc.* 261, 285 (2016).

Common-path versus Mach-Zehnder DHM systems

Highlights:

- **Robust** for highly dynamic imaging
- **Compact** and **portable** systems with minimum optical elements
- **Easily adaptable** to commercial microscopes as external modules
- **Low-cost** systems
- **Suitable for 3D printing**
- **Same imaging performance as two-beam interferometer DHM systems**

1
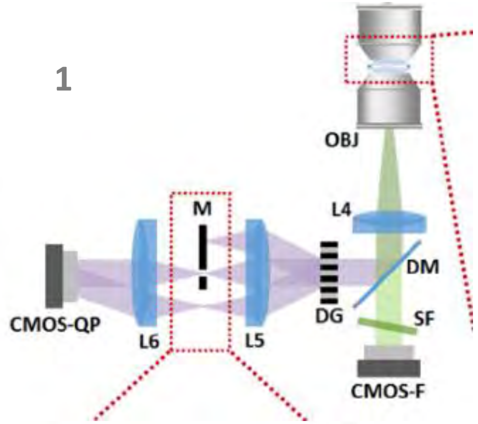

2
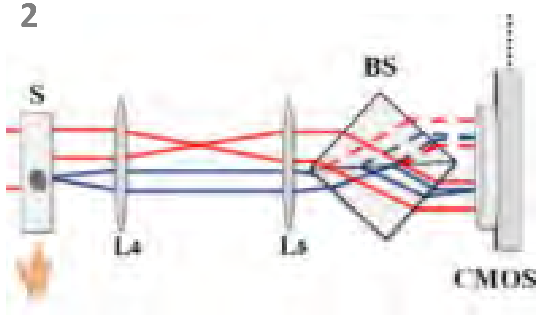

3
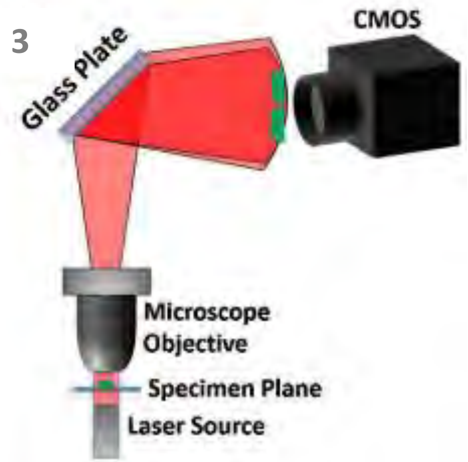

4
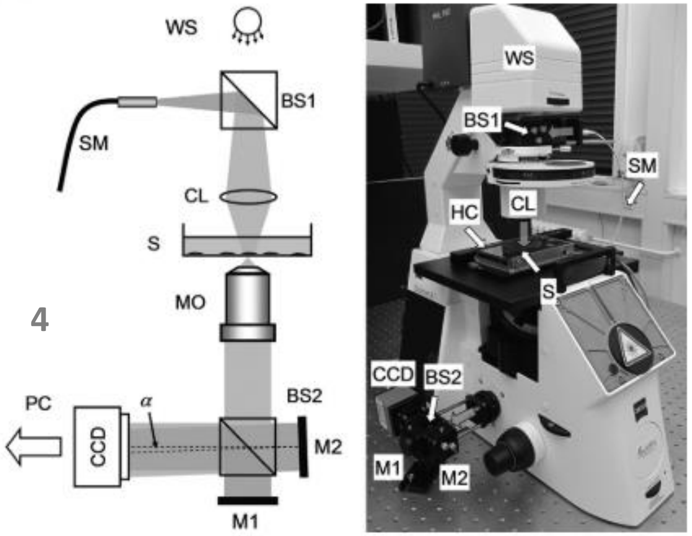

1. Chowdhury *et al.,* Biomed. Opt. Express 8, 2496 (2017)
2. Gabai *et al.,* Opt. Express 20, 26906 (2012)
3. Rawat, *et. al.*, Appl. Opt. 56, D127 (2017).
4. Kemper *et al.,* J. Biomed. Opt. 16, 026014 (2011).

Apparatus and Method to convert a regular bright-field microscope into a DHM system

Innovation: Introduction of a Fresnel biprism before the camera

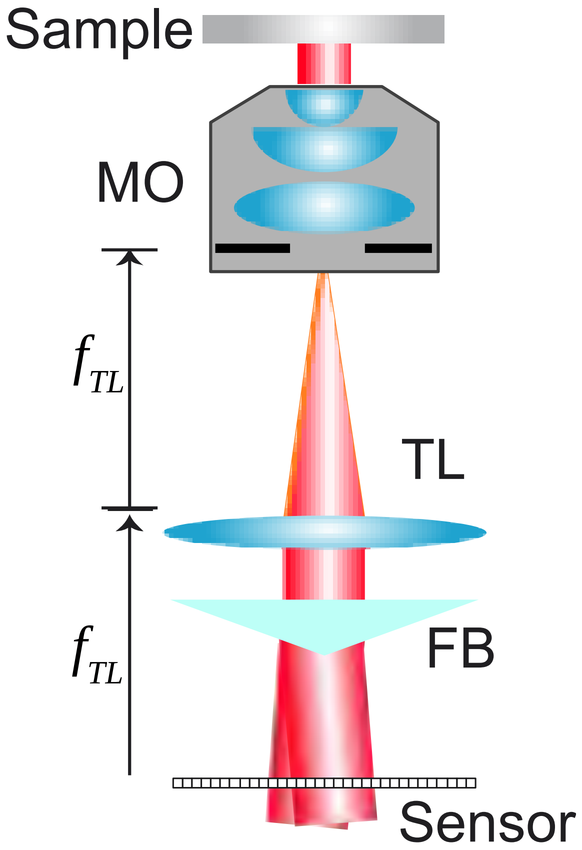

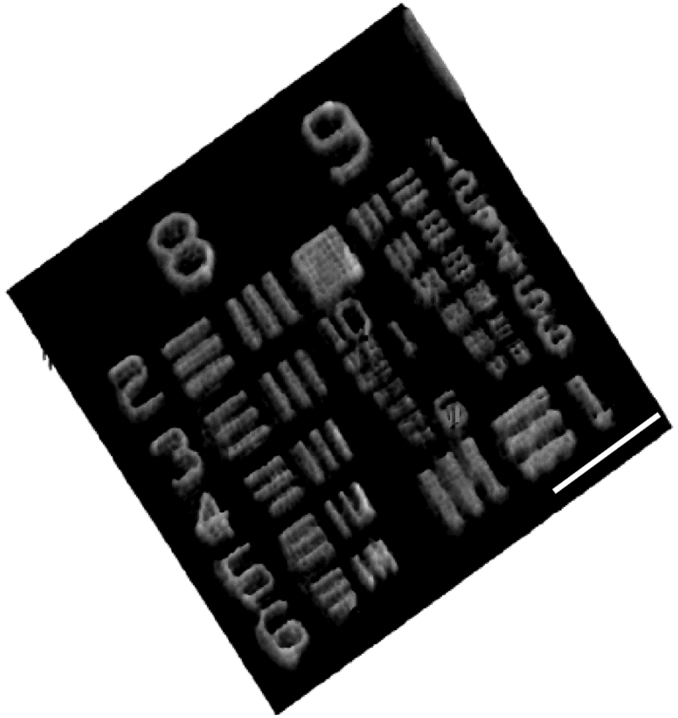

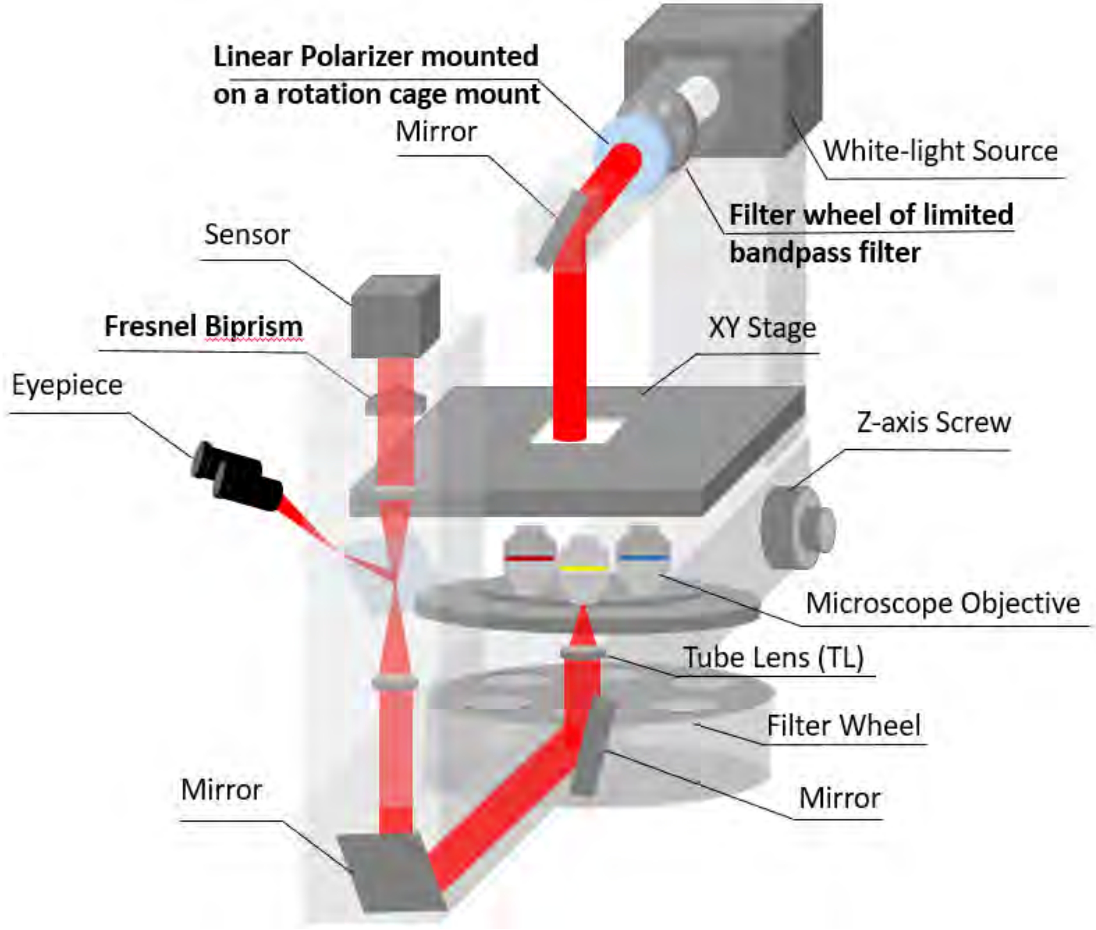

Hayes-Rounds & Doblas *et al.*, *JBO 25(8), 086501 (2020)*

Apparatus and Method to convert a regular bright-field microscope into a DHM system

Innovation Disclosure: Introduction of a Fresnel biprism before the camera

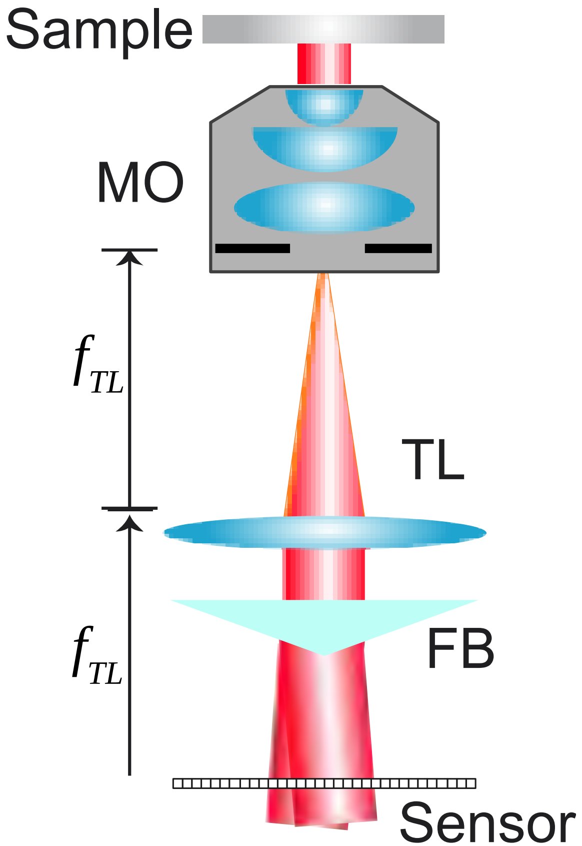

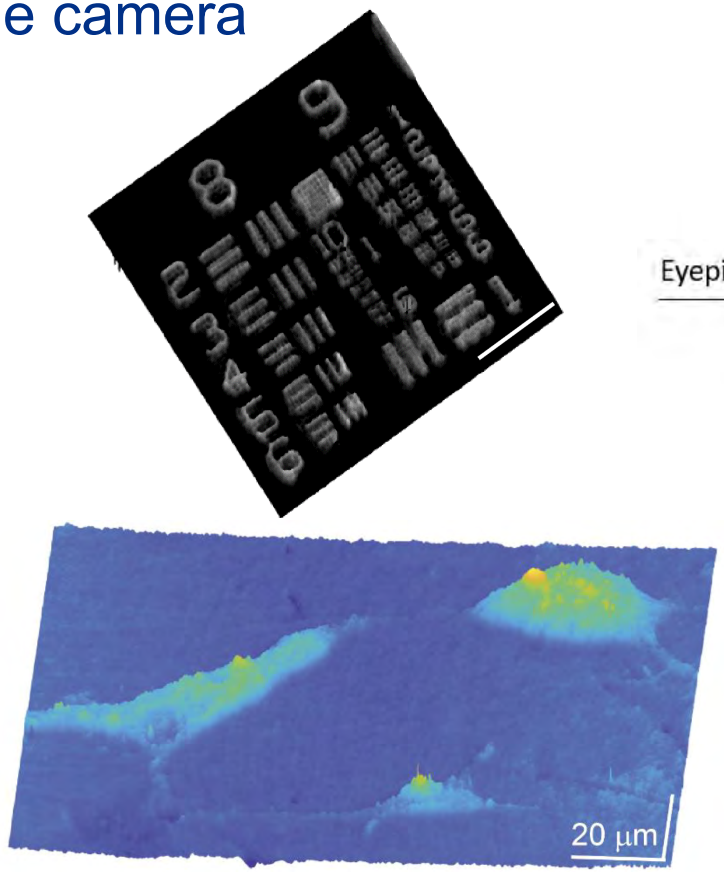

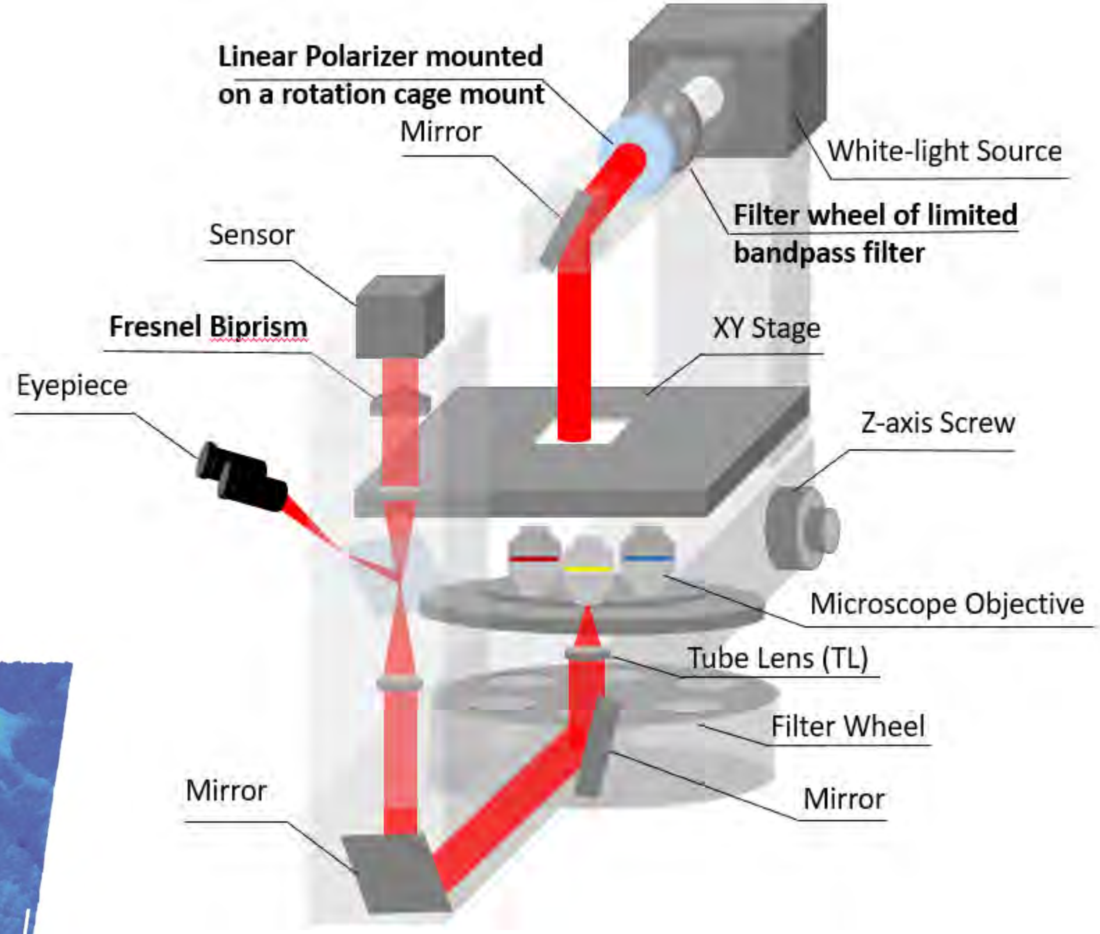

Hayes-Rounds & Doblas *et al.*, *JBO 25(8), 086501 (2020)*

Doblas *et al.*, US17/382,184 and WO/2022/020511

Novel Advantage of our Invention Disclosure versus another QPI-DHM patents

- Measurements of the **retardance map** of biological samples by adding **polarization sensitive capability** to the QPI-DHM technique.
- **More information** can be extracted from the biological samples by illuminating the sample at **different polarization states**.
- Among different applications, polarization-based measurements have **improved** the understanding of **biological processes** as well as the **classification** and **diagnosis** of cells/tissues.

Human U87 glioblastoma cells

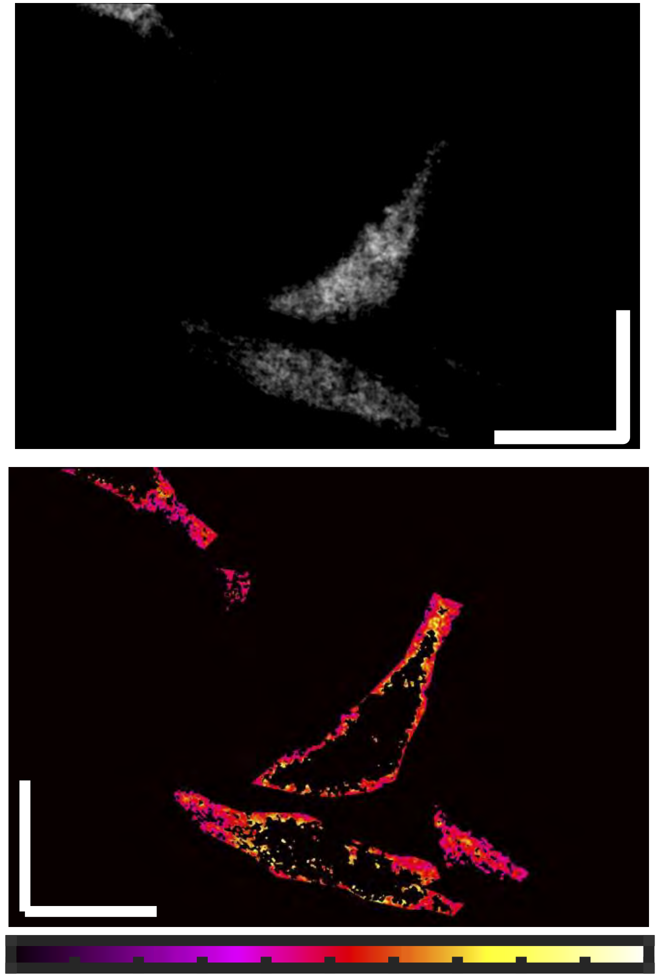

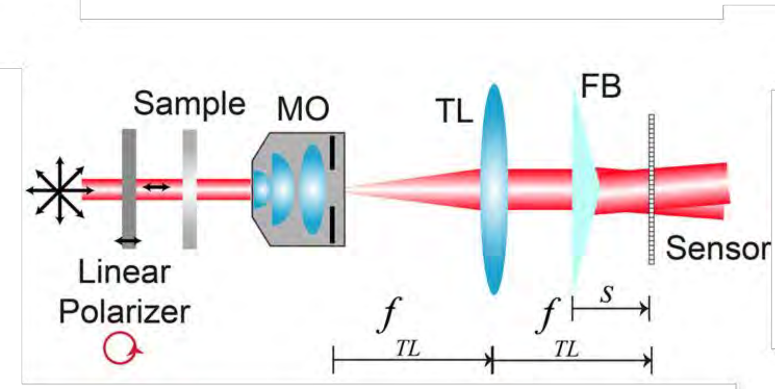

Hayes-Rounds & Doblas *et al., JBO 25(8), 086501 (2020)*

Systems with Polarization-Sensitive Capability shows a huge potential for cancer research studies

Bright-field microscope

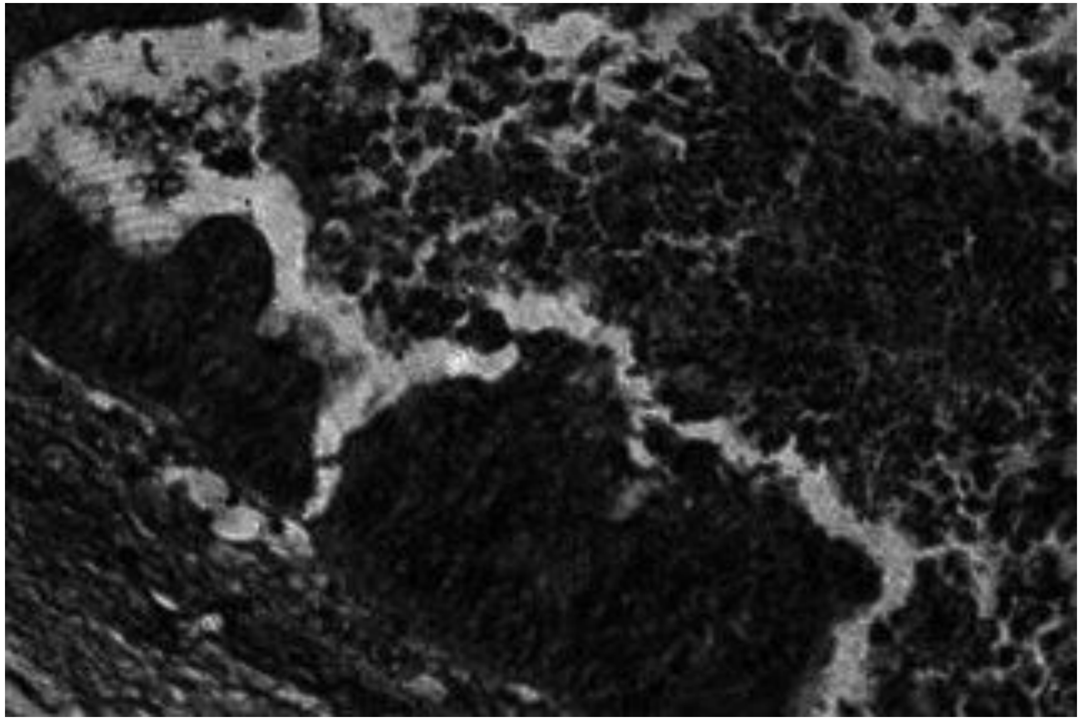

Retardance Map

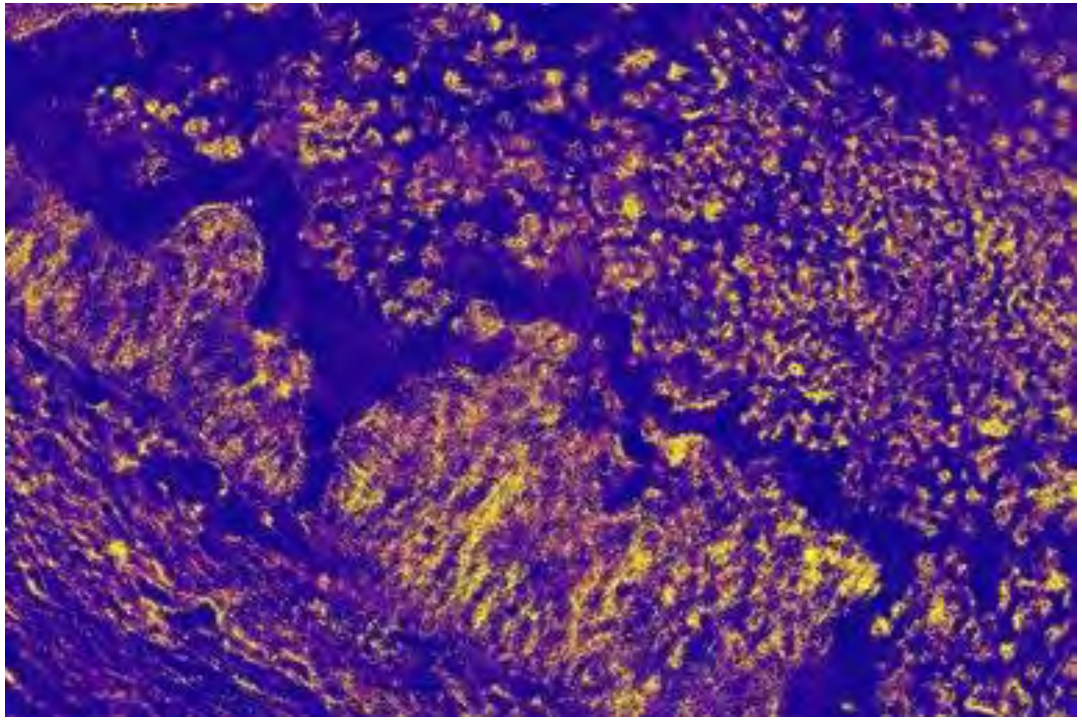

Adenocarcinoma of ovary

Obando-Vasquez & Doblas *et al.*, American Journal of Physics 90, 702 (2022). doi: 10/1119/5.0081673

The major limitation of the common-path DHM systems is their restriction to spatially sparse samples

Restriction: $M_1\Delta_x \leq L/2$

Common-path DHM systems are based on the **self-interference** of **two laterally-displaced replicas of the object image**

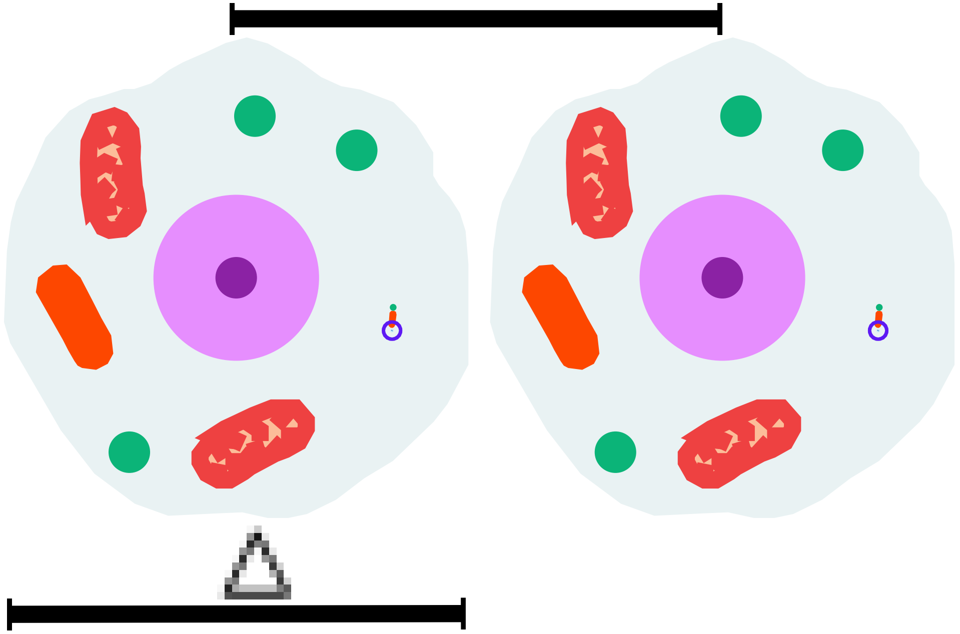

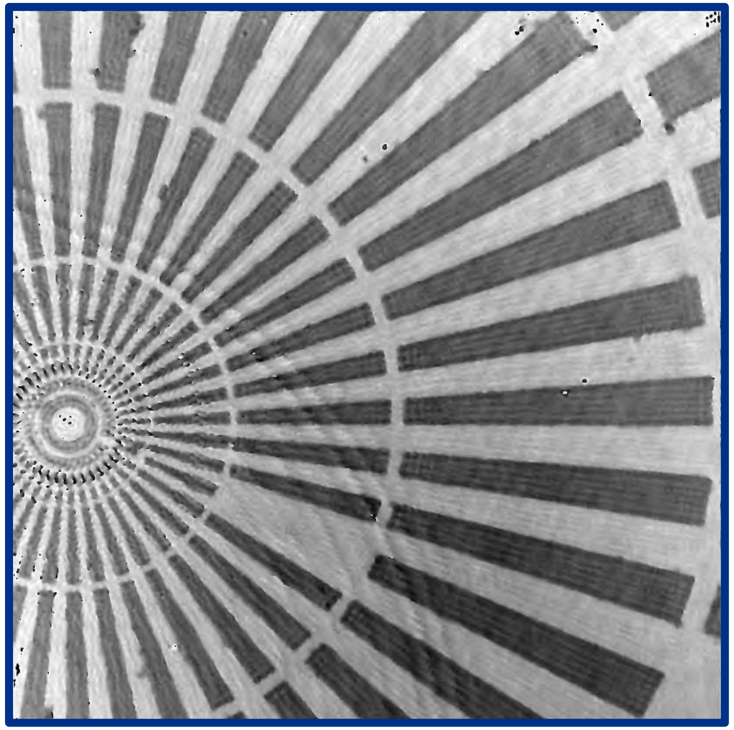

M_1 – Lateral Magnification **Δ_x** – Sample Size

L/2 – Lateral Separation of object replicas

The major limitation of the common-path DHM systems is their restriction to spatially sparse samples

Increasing the lateral magnification may produce a spatial overlay between the two object replicas

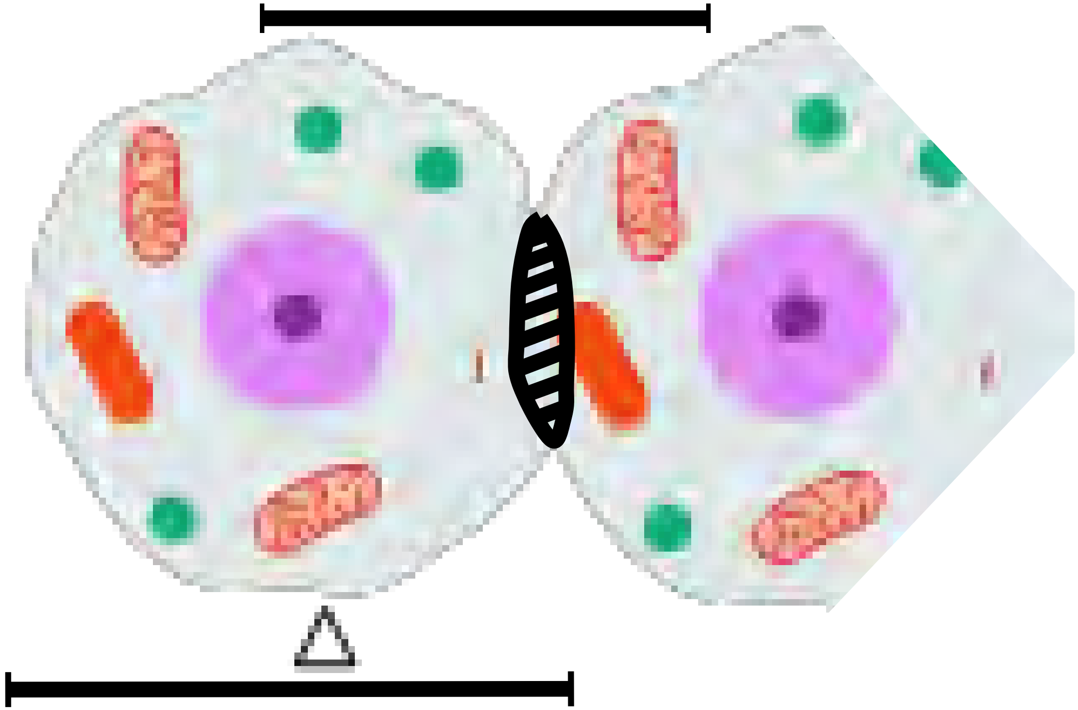

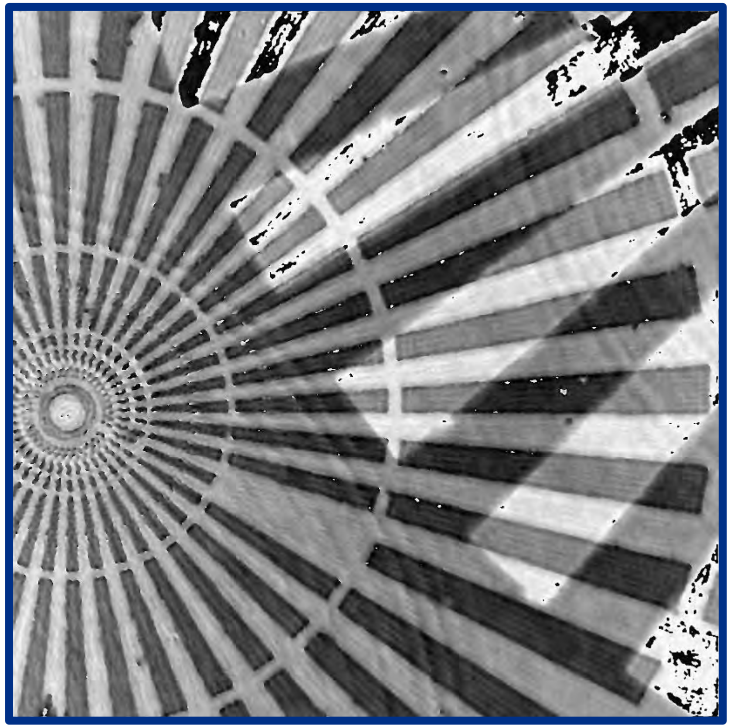

M_2 – Lateral Magnification **Δ_x** – Sample Size
L/2 – Lateral Separation of object replicas

Common-path DHM using a Fresnel biprism for spatially dense microscopic samples

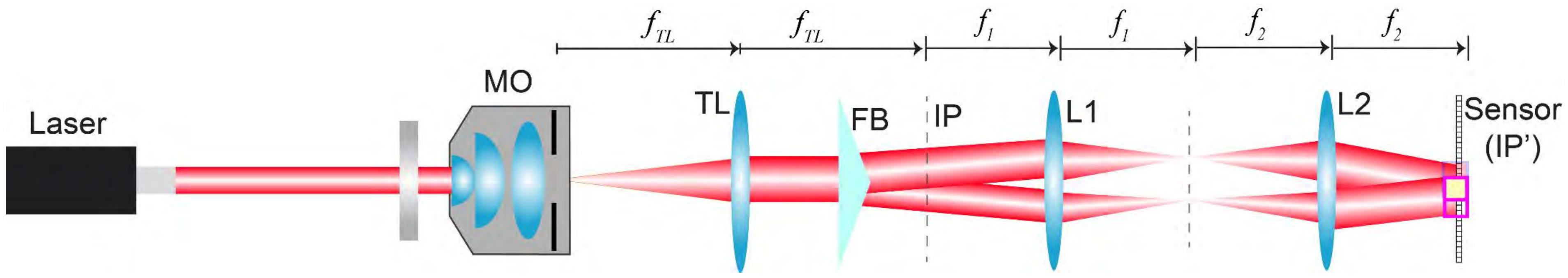

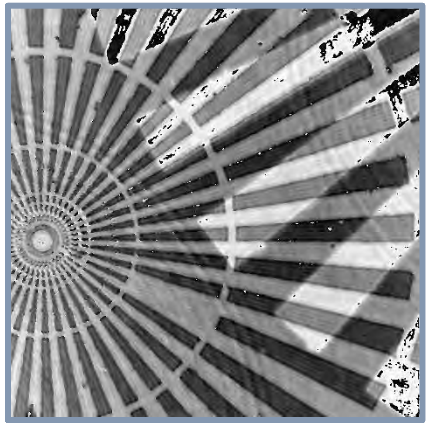

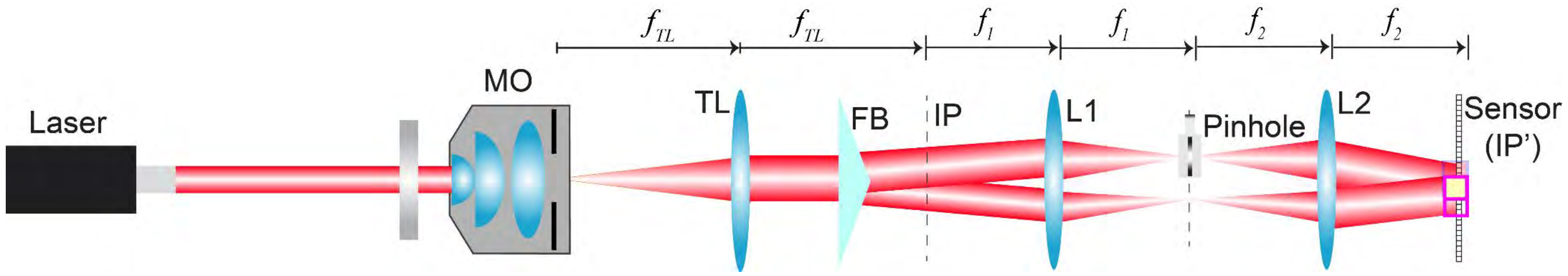

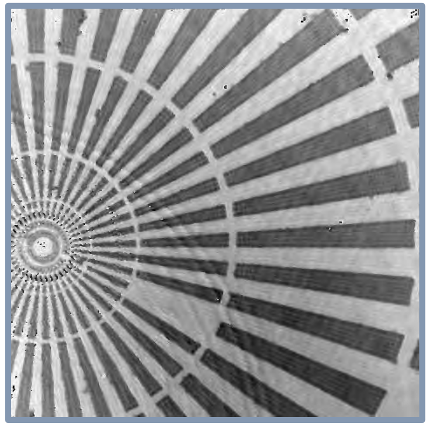

FB – Fresnel Biprism **IP** – Image Plane **L** – Lens

MO – Objective lens **TL** – Tube lens

Doblas *et al.*, *Sensors 22*, 3793 (2022).

The pinhole size controls the frequency content of one of the object replicas

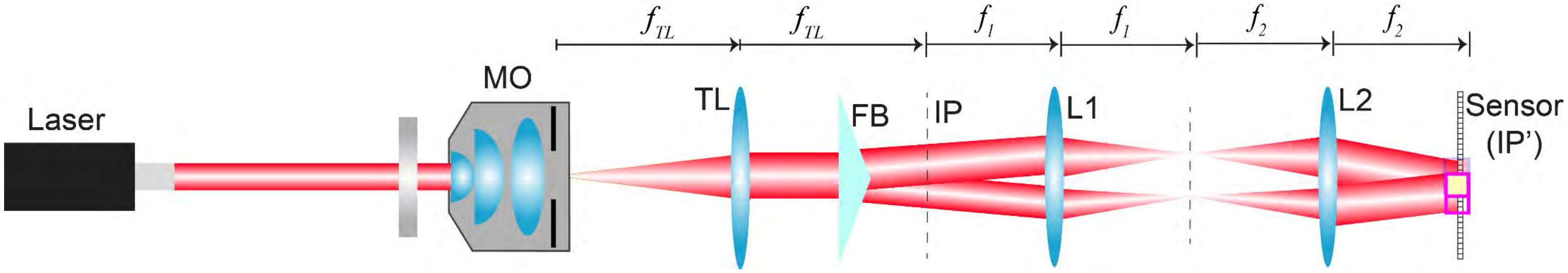

FB – Fresnel Biprism
IP – Image Plane
L – Lens
MO – Objective lens
TL – Tube lens

The pinhole size controls the frequency content of one of the object replicas

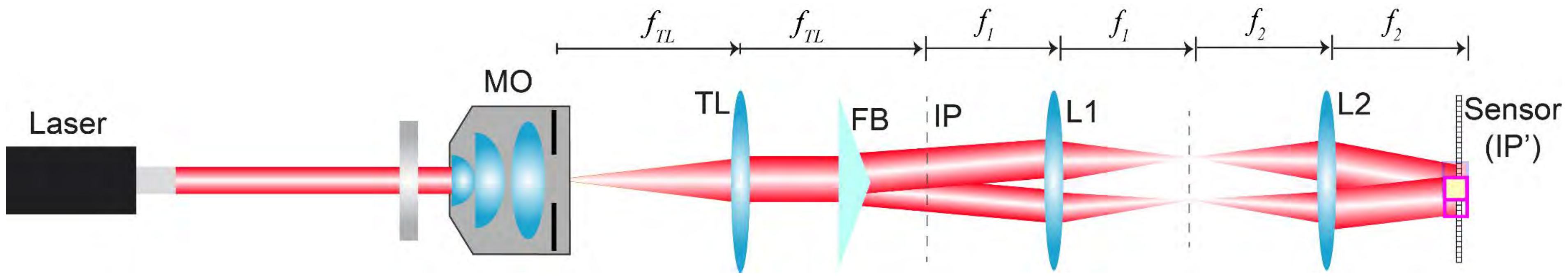

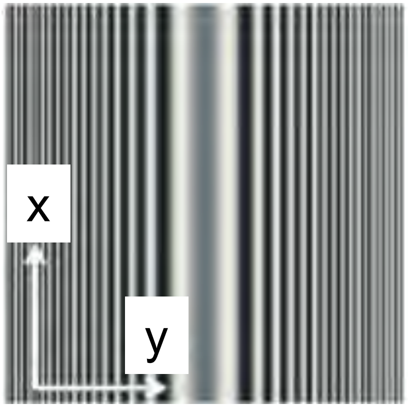

IP

FB – Fresnel Biprism
IP – Image Plane
L – Lens
MO – Objective lens
TL – Tube lens

The pinhole size controls the frequency content of one of the object replicas

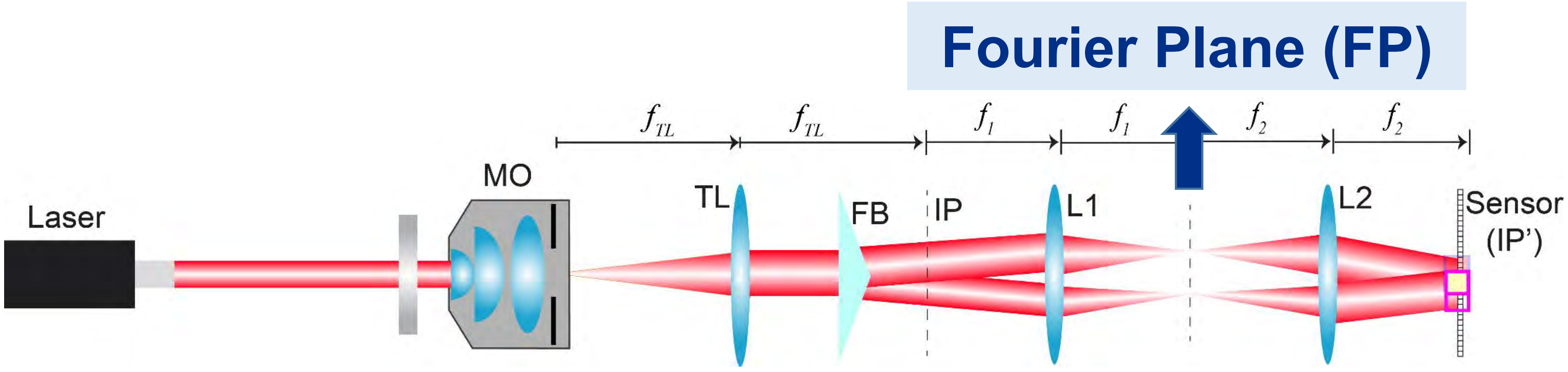

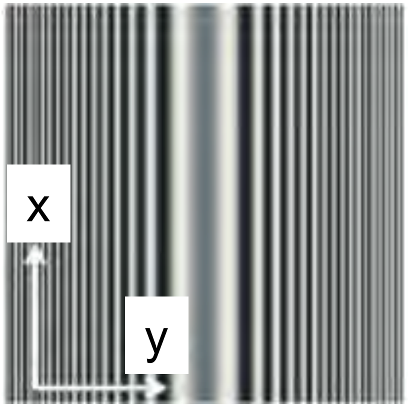

IP

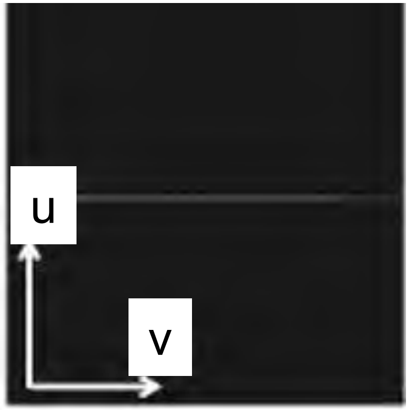

FP

FB – Fresnel Biprism
IP – Image Plane
L – Lens
MO – Objective lens
TL – Tube lens

The pinhole size controls the frequency content of one of the object replicas

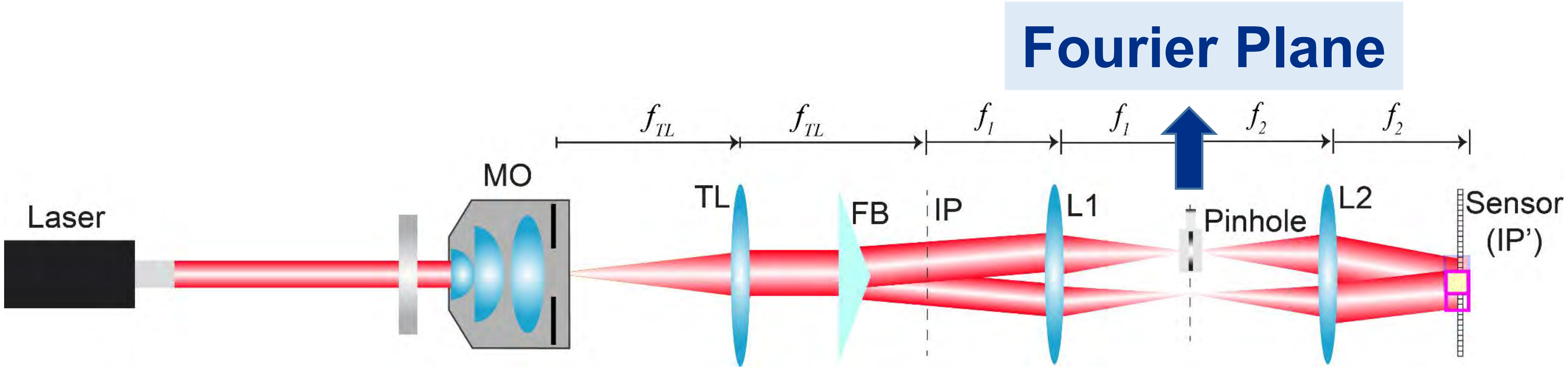

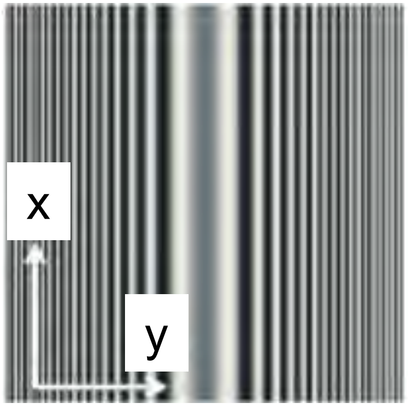

IP

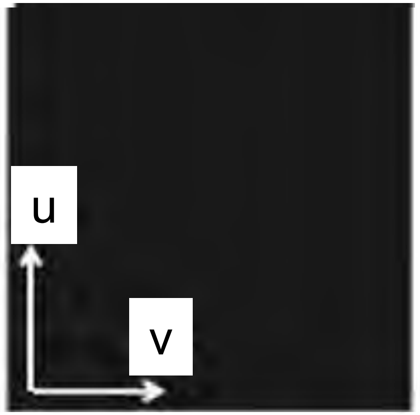

FP

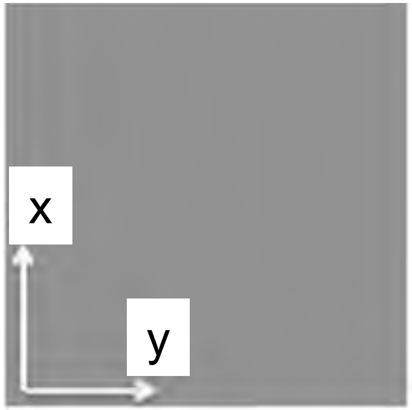

IP'

FB – Fresnel Biprism
IP – Image Plane
L – Lens
MO – Objective lens
TL – Tube lens

Common-path dual-mode DHM using a Fresnel biprism for transmissive and reflective samples

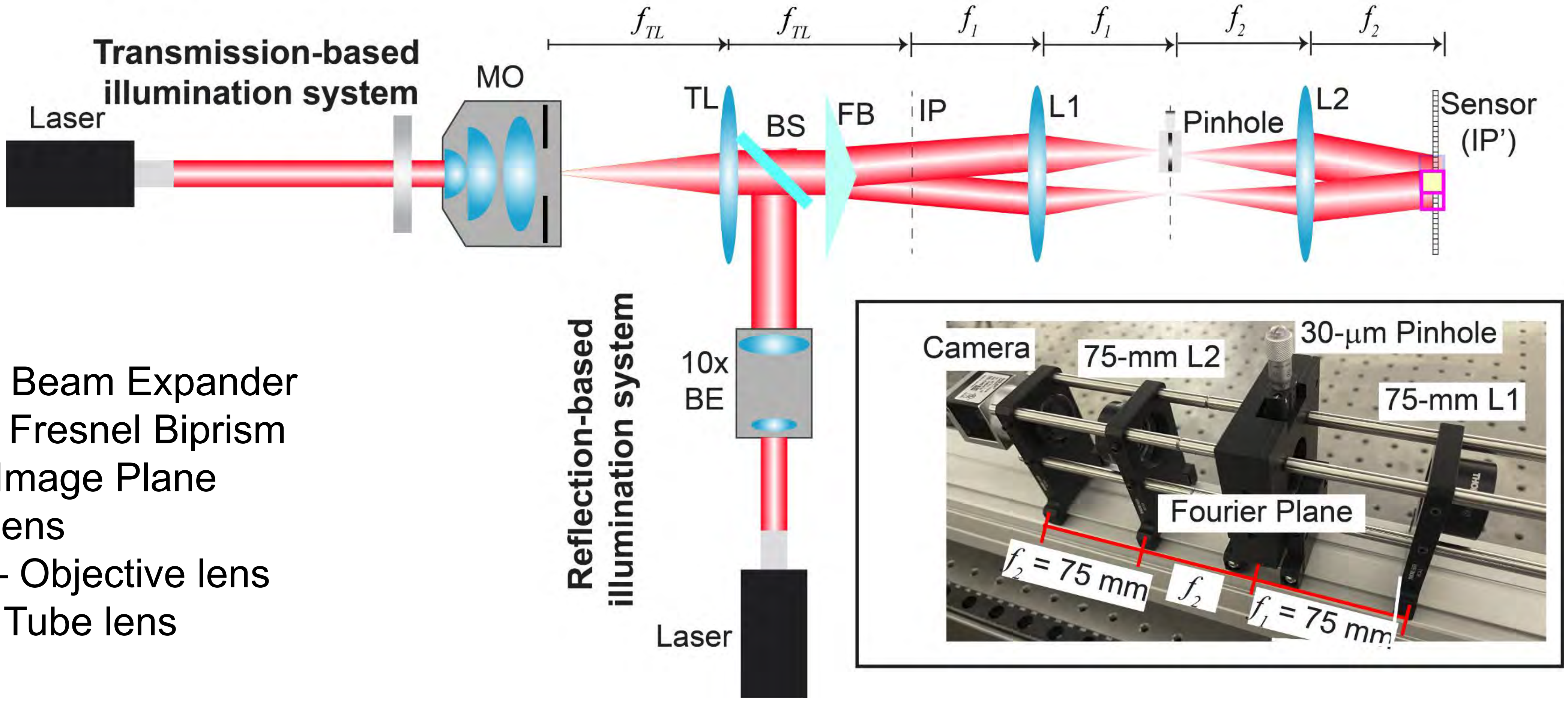

BE – Beam Expander
FB – Fresnel Biprism
IP – Image Plane
L – Lens
MO – Objective lens
TL – Tube lens

Doblas *et al.*, *Sensors 22*, 3793 (2022).

Common-path dual-mode DHM using a Fresnel biprism for transmissive and reflective samples

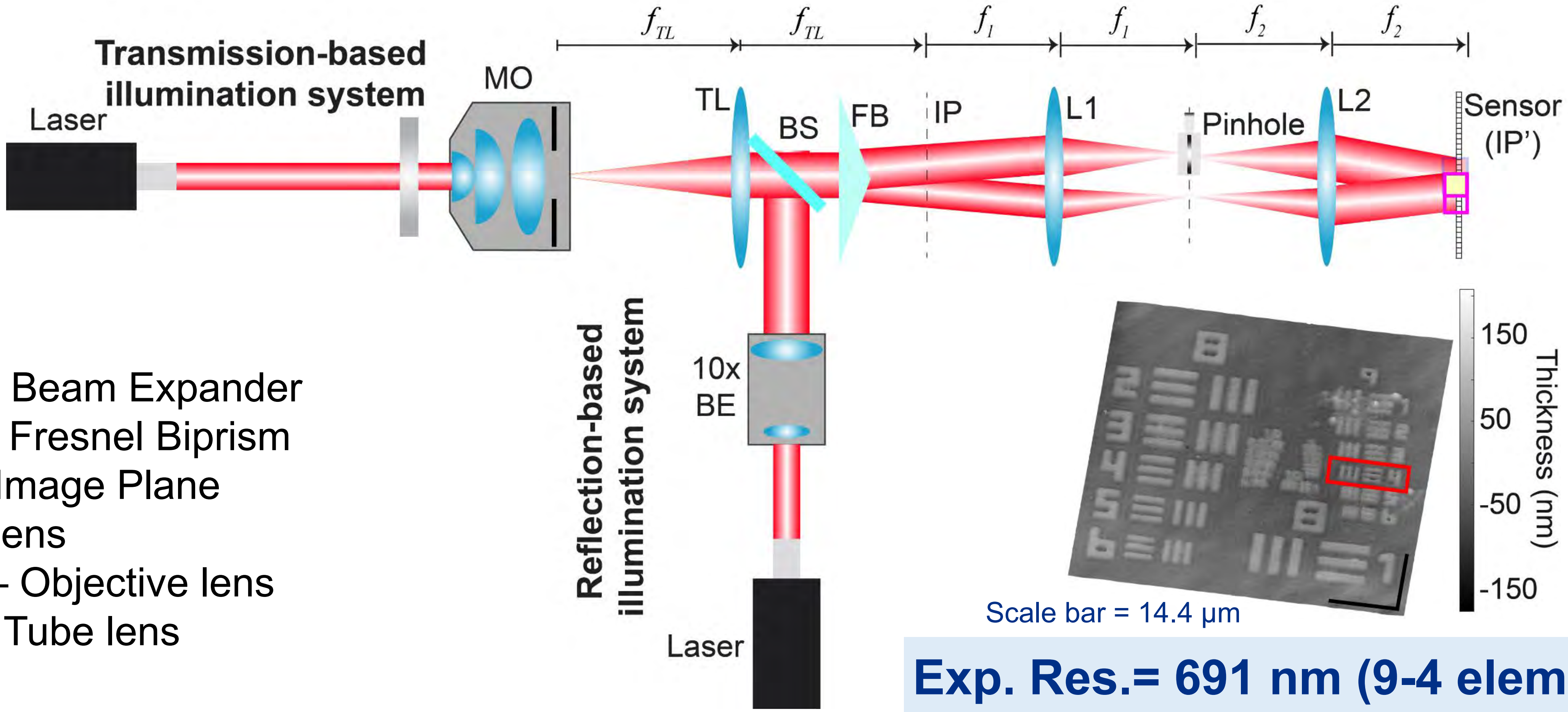

Scale bar = 14.4 μm

BE – Beam Expander
FB – Fresnel Biprism
IP – Image Plane
L – Lens
MO – Objective lens
TL – Tube lens

Exp. Res.= 691 nm (9-4 element)
Theo. Res. = 709 nm
(e.g., λ/NA = 532 nm/0.75)

Doblas *et al.*, *Sensors 22*, 3793 (2022).

The dual-mode FB-based DHM system has better resolution than a commercial profilometer

Reconstructed Phase Images of a reflective USAF target

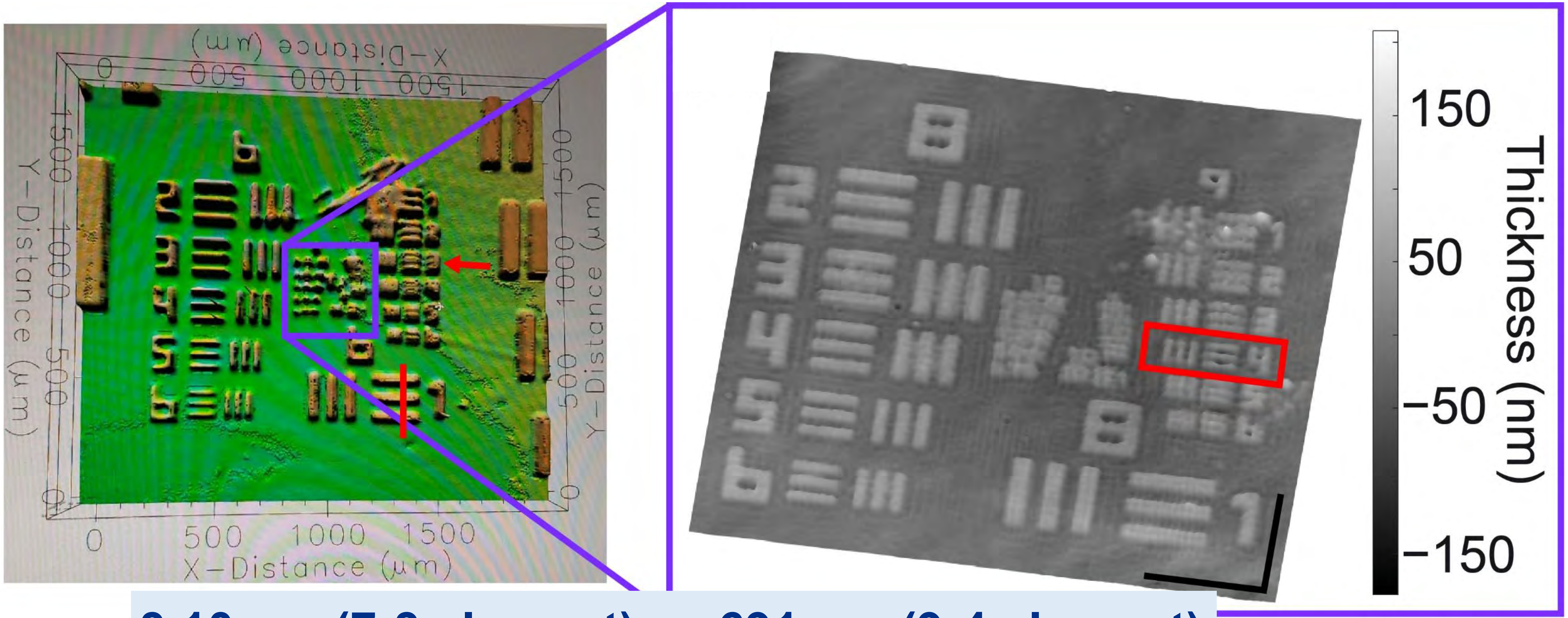

3.10 µm (7-3 element) vs 691 nm (9-4 element)

THE UNIVERSITY OF MEMPHIS

Doblas *et al.*, *Sensors* 22, 3793 (2022).

Module Commercial device

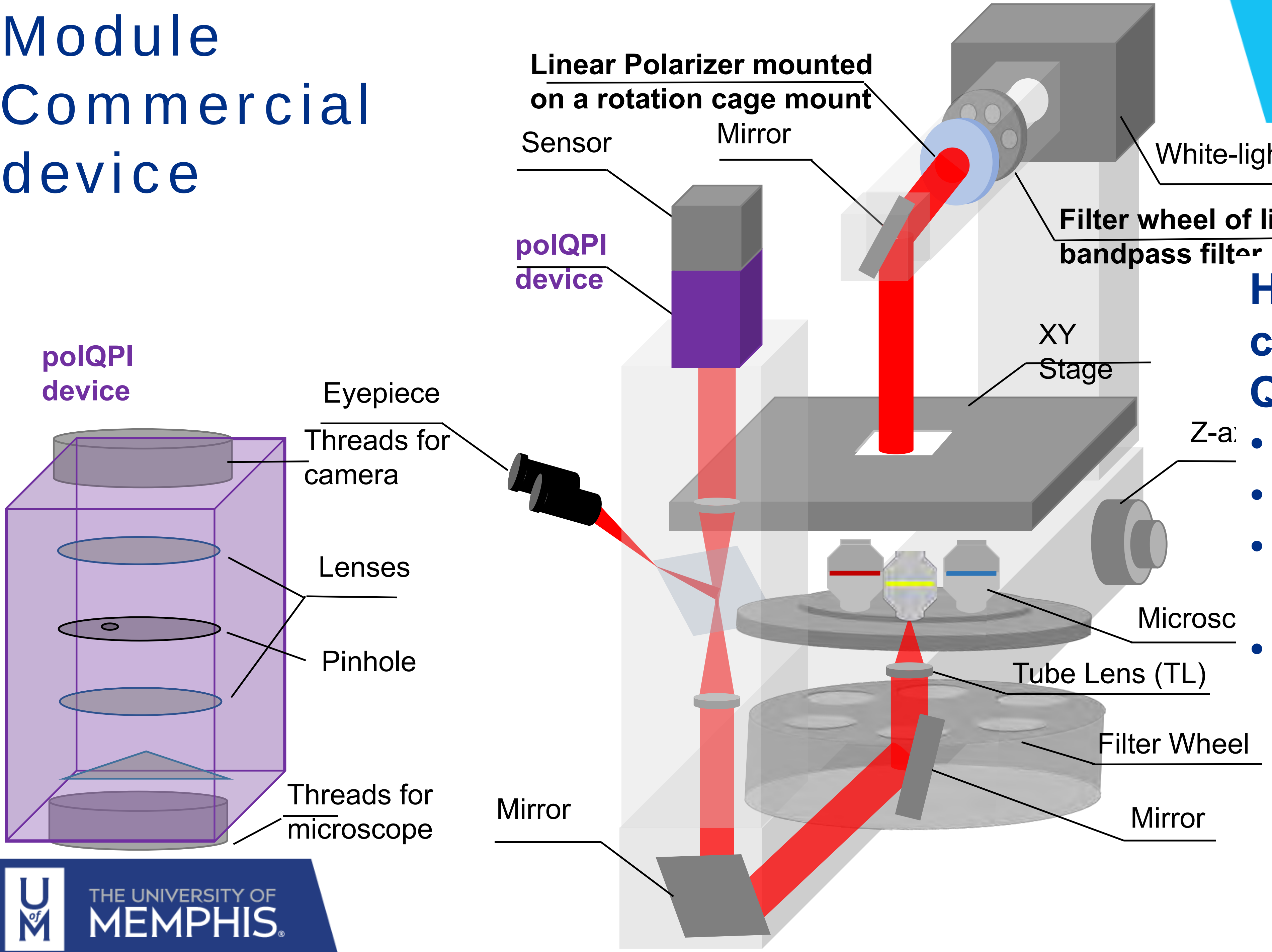

Hallmark over current commercial QPI systems

- External module
- Minimum elements
- Polarization Sensitive
- Low-cost device

Future of DHM as STEM Toys Market

- High demand of STEM education toys that support academics, in particular the 8-12 age group.
- STEM market expected to grow by 7% annually to a market of $9.5 Billion by 2025
- Features of the potential polDHM STEM toys: improve of motor skills and cognitive development and demand for coding.
- What can we offer? A low-cost (<$200) DHM microscope with 3D printed mounts and a Raspberry Pi camera. Students will learn Optics laws, Electronics and Coding.

STEM Toys Market, *Research and Markets, (2019)*

Innovations in the reconstruction method relies on the development of a robust and automatic method

FT Hologram: $H(\mathbf{u}) = DC(\mathbf{u}) + U(\mathbf{u}) \otimes_2 \delta(\mathbf{u}-\mathbf{k}) + U^*(\mathbf{u}) \otimes_2 \delta(\mathbf{u}+\mathbf{k})$

Spatial Filtering

$H_F(\mathbf{u}) = U_{IP}(\mathbf{u}) \otimes_2 \delta(\mathbf{u}-\mathbf{k})$

Ref. Compensation

$H(\mathbf{u}) \otimes_2 R(\mathbf{u}) = U_{IP}(\mathbf{u})$

FT^{-1}

$u_{IP}(\mathbf{x})$

Amplitude-contrast

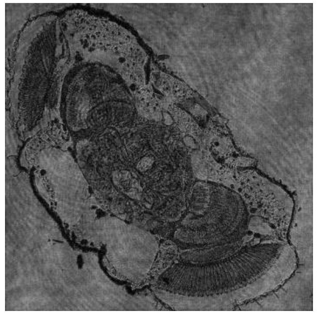

$a(\mathbf{x}) = \sqrt{|u_{IP}(\mathbf{x})|^2}$

Phase-contrast

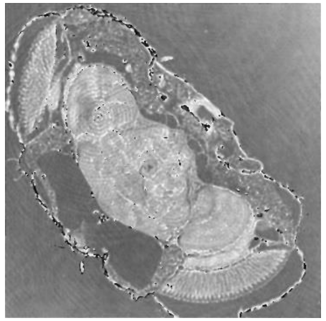

$\varphi(\mathbf{x}) = \text{atan}\left[\frac{\text{Im}(u_{IP})}{\text{Re}(u_{IP})}\right]$

KEY STEP FOR ACCURATE QPI

THE UNIVERSITY OF MEMPHIS

Requirement of the generation of a digital reference beam for QPI measurements

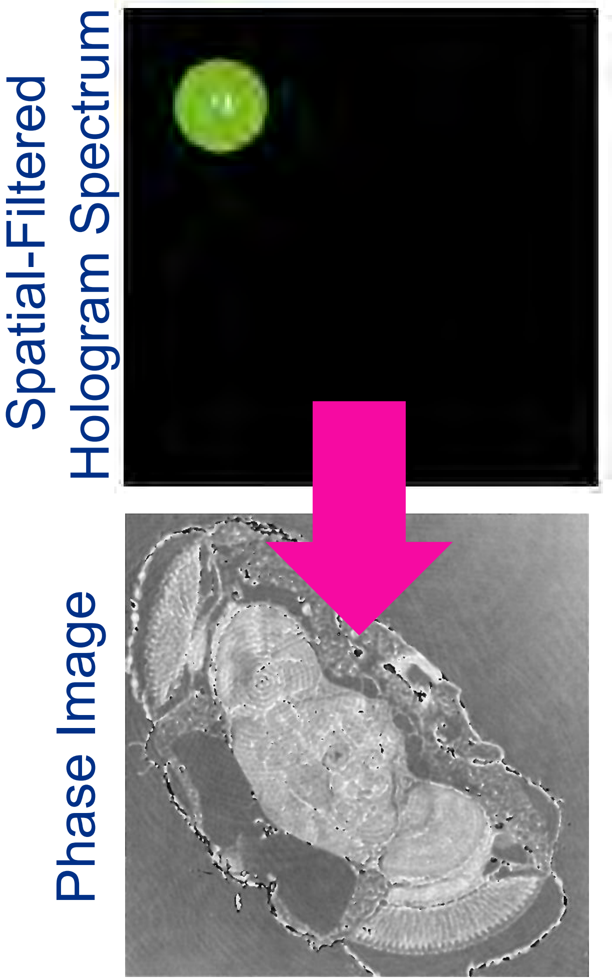

1. Inverse FT of the filtered hologram spectrum $h_F(\boldsymbol{x})$
2. Generation of a digital reference wave

$$r_D(m,n)=\sum_{m,n}\exp\left[\,\mathrm{i}\frac{2\pi}{\lambda}\left(m\bullet\sin\theta_x\bullet M+n\bullet\sin\theta_y\bullet N\right)\Delta_{\mathrm{xy}}\right]$$

(M,N) → size of the reconstructed image

Δ_{xy} → square pixel size

(m,n) → index pixel position

λ → ’ w

Requirement of the generation of a digital reference beam for QPI measurements

Spatial-Filtered Hologram Spectrum

Phase Image

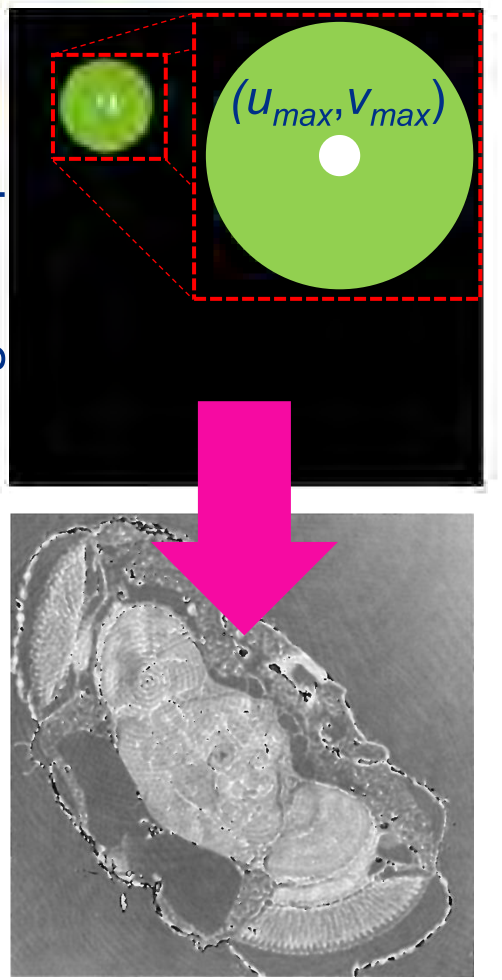

1. Inverse FT of the filtered hologram spectrum $h_F(\boldsymbol{x})$
2. Generation of a digital reference wave

$$r_D(m,n) = \sum_{m,n} \exp\left[i \frac{2\pi}{\lambda} \left(m \bullet \sin\theta_x \bullet M + n \bullet \sin\theta_y \bullet N \right) \Delta_{xy} \right]$$

Reference angle, $\boldsymbol{\theta} = (\theta_x, \theta_y)$, is provided by the pixel position of max value peak for the order +1, (u_{max}, v_{max})

$$\theta_x = \sin^{-1}\left(\frac{|u_0 - u_{max}|\lambda}{M\Delta_{xy}} \right) \qquad \theta_y = \sin^{-1}\left(\frac{|v_0 - v_{max}|\lambda}{N\Delta_{xy}} \right)$$

(M,N) → size of the reconstructed image
(m,n) → index pixel position
λ → ' w

Δ_{xy} → square pixel size
$(u_0,v_0) = (M/2+1, N/2+1)$ → pixel position of the DC term
(u_{max},v_{max}) → max peak pixel position of the +1 term

Requirement of the generation of a digital reference beam for QPI measurements

Spatial-Filtered Hologram Spectrum

Phase Image

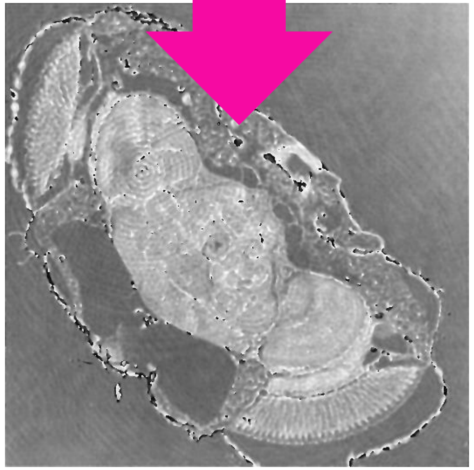

1. Inverse FT of the filtered hologram spectrum $h_F(\boldsymbol{x})$
2. Generation of a digital reference wave

$$r_D(m,n) = \sum_{m,n} \exp\left[\mathrm{i}\frac{2\pi}{\lambda}\left(m \bullet \sin\theta_x \bullet M + n \bullet \sin\theta_y \bullet N\right)\Delta_{\mathrm{xy}} \right]$$

3. Complex object information without distortion of the reference beam

$$\hat{o}(\boldsymbol{x}) = r_D(\boldsymbol{x}) \bullet h_F(\boldsymbol{x})$$

(M,N) → size of the reference image
Δxy → square pixel size
(m,n) → index pixel position
λ → ’ w

THE UNIVERSITY OF MEMPHIS

Requirement of the generation of a digital reference beam for QPI measurements

Spatial-Filtered Hologram Spectrum

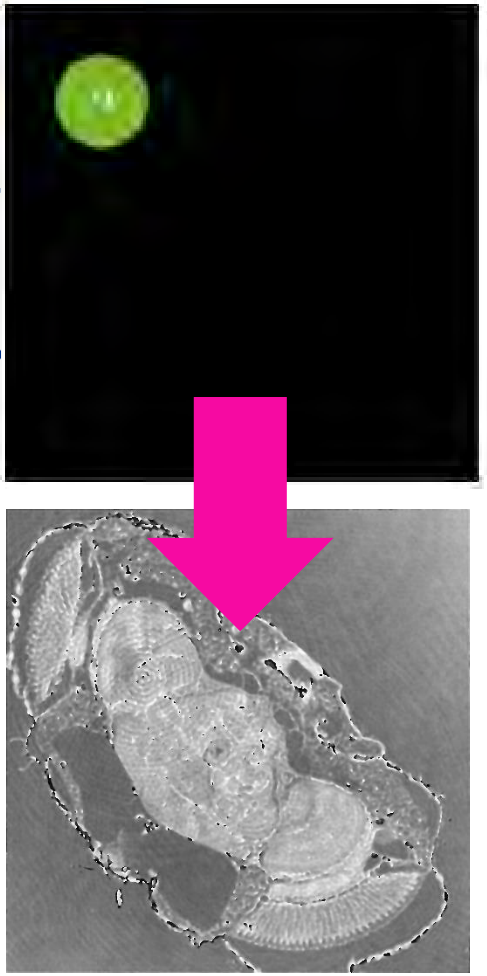

Phase Image

1. Inverse FT of the filtered hologram spectrum $h_F(\boldsymbol{x})$
2. Generation of a digital reference wave

$$r_D(m,n) = \sum_{m,n} \exp\left[i \frac{2\pi}{\lambda} \left(m \bullet \sin\theta_x \bullet M + n \bullet \sin\theta_y \bullet N \right) \Delta_{xy} \right]$$

3. Complex object information without distortion of the reference beam

$$\hat{o}(\boldsymbol{x}) = r_D(\boldsymbol{x}) \bullet h_F(\boldsymbol{x})$$

4. Estimation of the phase map

$$\hat{\varphi}(\boldsymbol{x}) = \tan^{-1}\left(\frac{\mathrm{Im}\left[\hat{o}(\boldsymbol{x})\right]}{\mathrm{Re}\left[\hat{o}(\boldsymbol{x})\right]} \right)$$

(M,N) → size of the reconstructed image

(m,n) → index pixel position

λ → ' w

Δ_{xy} → square pixel size

Need for correct estimation of the position of the maximum peak of the +1 term

T w b ’ w λ), the features of the digital sensor *(M, N, Δ_{xy})* and the subtraction between the pixel positions of the DC and +1 terms

$$\theta_x = \sin^{-1}\left(\frac{|u_0 - u_{max}|\lambda}{M\Delta_{xy}}\right) \qquad \theta_y = \sin^{-1}\left(\frac{|v_0 - v_{max}|\lambda}{N\Delta_{xy}}\right)$$

Need for correct estimation of the position of the maximum peak of the +1 term

T w b ’ w λ), the features of the digital sensor *(M, N, Δ_{xy})* and the subtraction between the pixel positions of the DC and +1 terms

$$\theta_x = \sin^{-1}\left(\frac{\left|u_0 - u_{max}\right|\lambda}{M\Delta_{xy}}\right) \qquad \theta_y = \sin^{-1}\left(\frac{\left|v_0 - v_{max}\right|\lambda}{N\Delta_{xy}}\right)$$

Filtered hologram spectrum: H_F

(u_{max}, v_{max}) = integer values (IDEAL CASE)

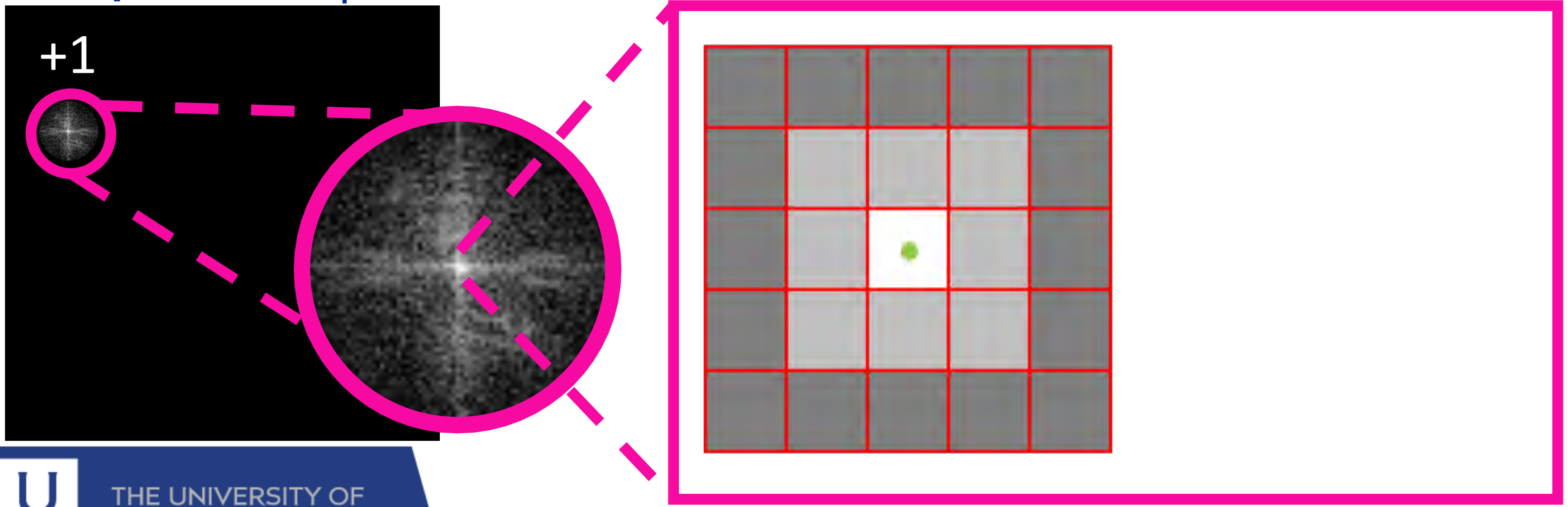

Need for correct estimation of the position of the maximum peak of the +1 term

T w b ’ w λ), the features of the digital sensor *(M, N, Δ_{xy})* and the subtraction between the pixel positions of the DC and +1 terms

$$\theta_x = \sin^{-1}\left(\frac{|u_0 - u_{max}|\lambda}{M\Delta_{xy}}\right) \qquad \theta_y = \sin^{-1}\left(\frac{|v_0 - v_{max}|\lambda}{N\Delta_{xy}}\right)$$

Filtered hologram spectrum: H_F

(u_{max}, v_{max}) = non-integer values (REAL CASE)

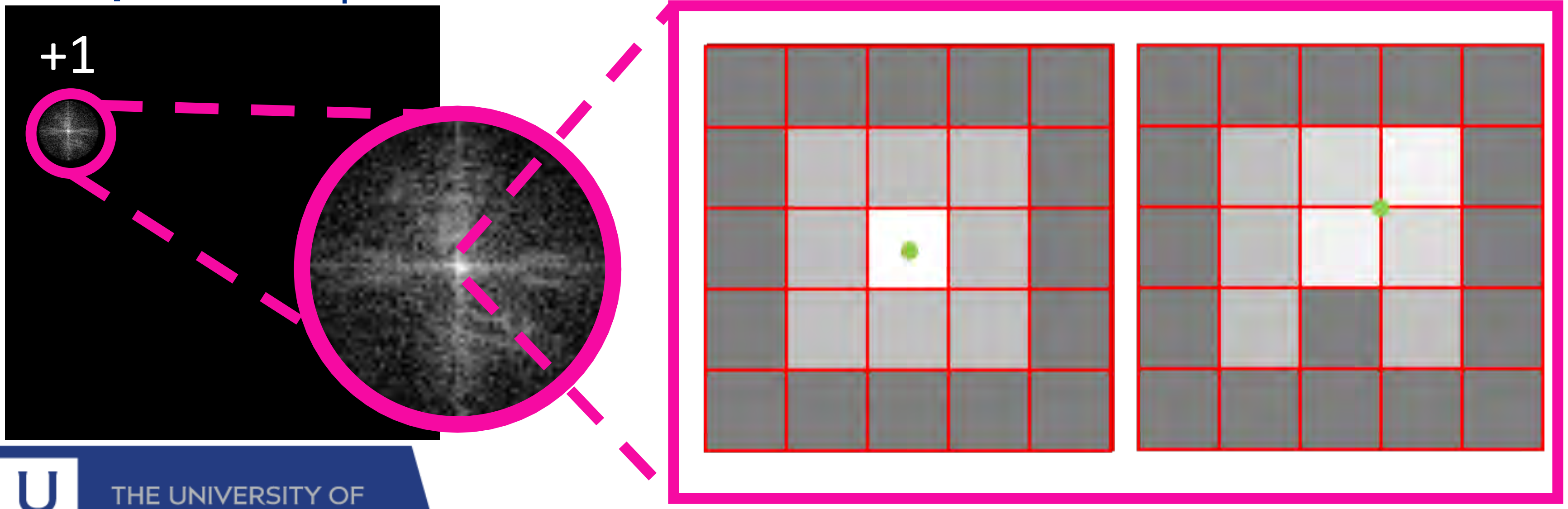

Distorted phase image if one uses the wrong values of (u_{max}, v_{max})

Best/Optimal Reconstructed Phase Image

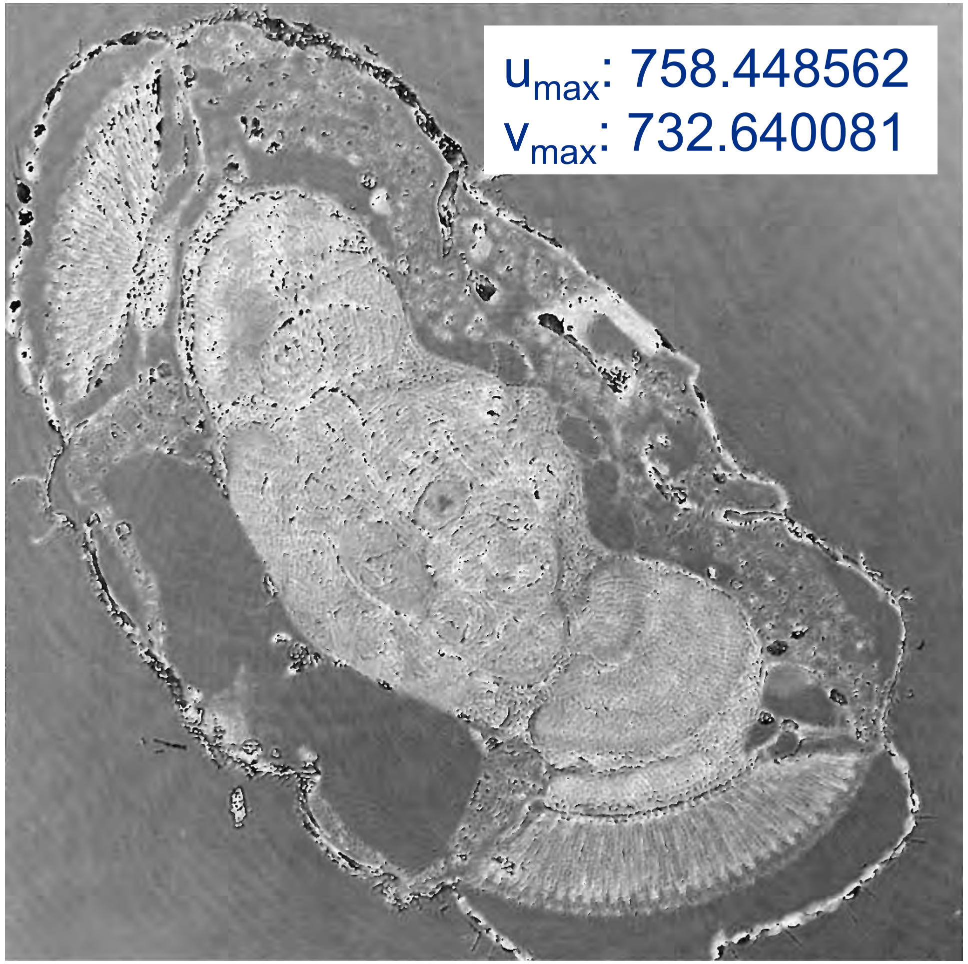

Non-Optimal Reconstructed Phase Image

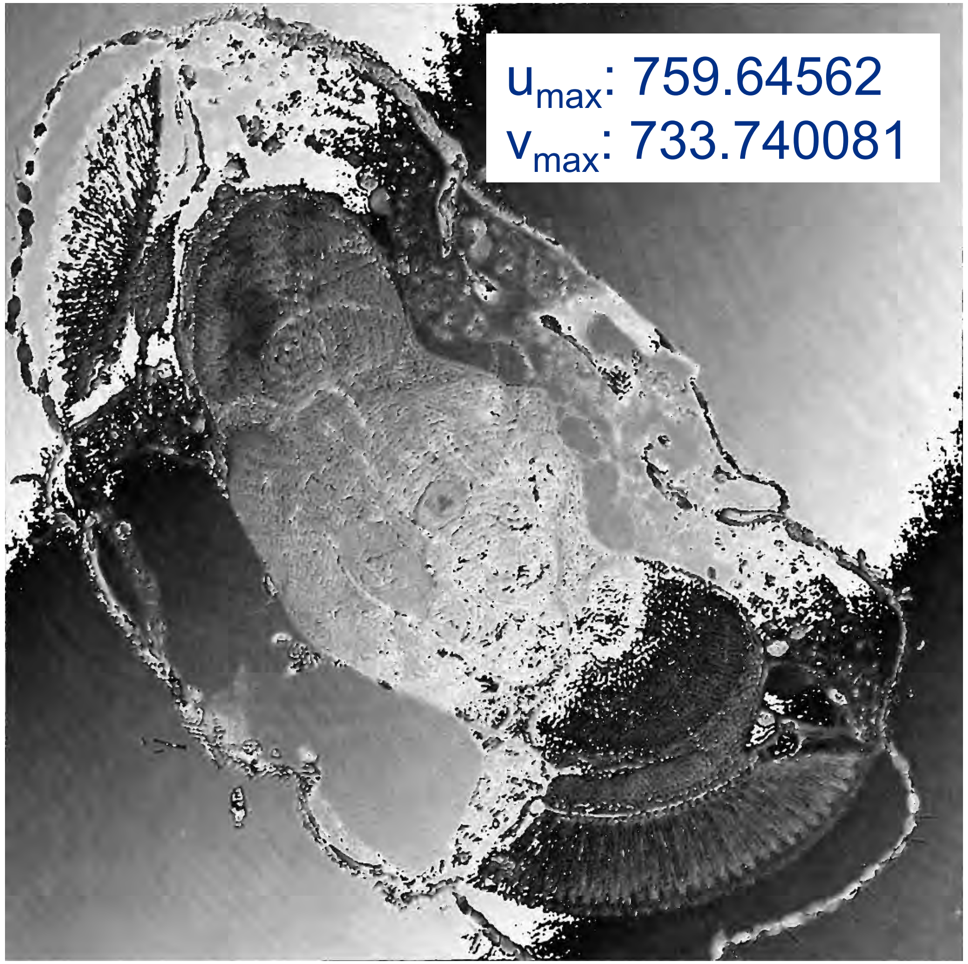

The best reconstructed phase image contains the smaller number of phase jumps

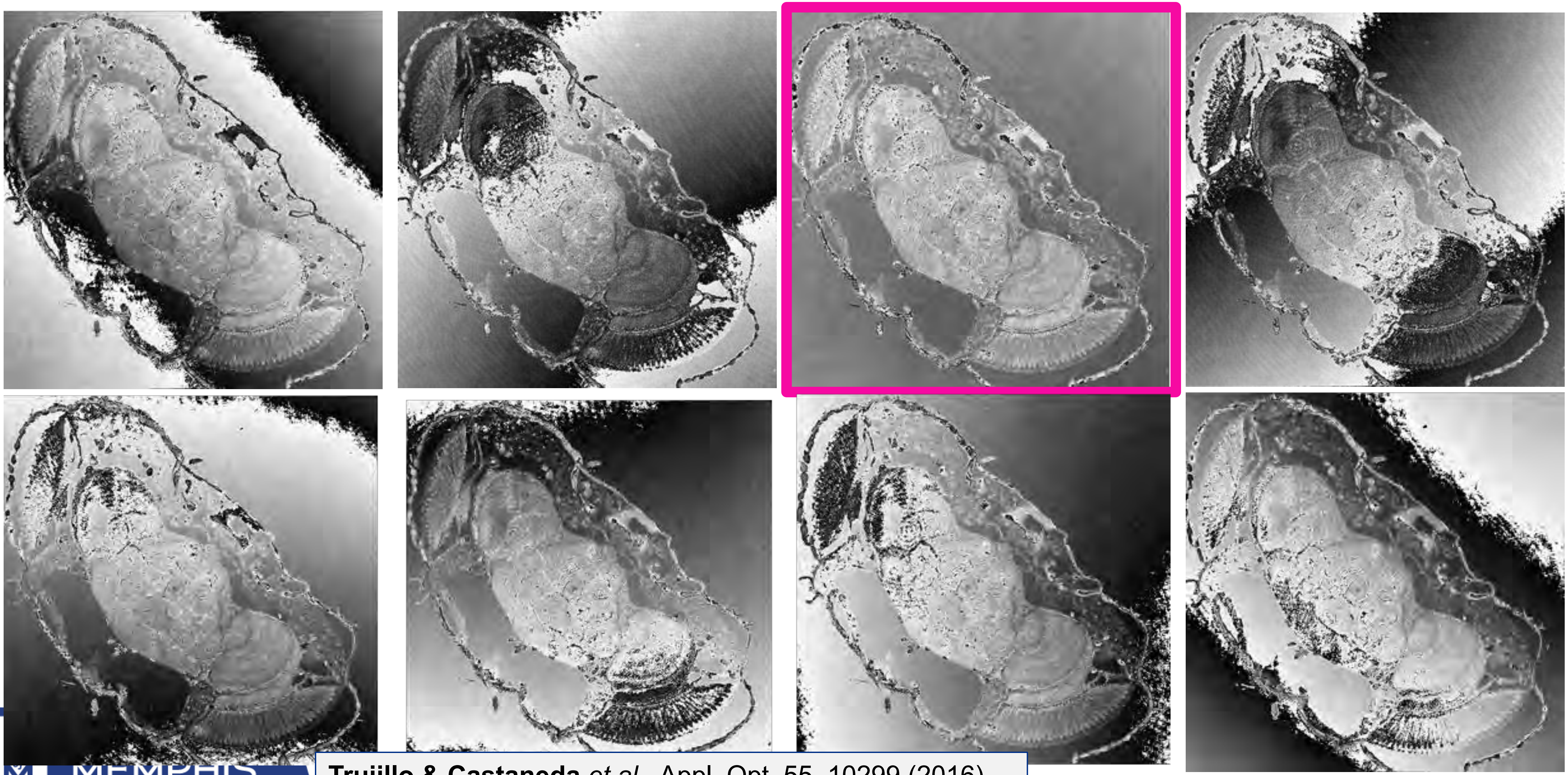

Trujillo & Castaneda *et al.*, Appl. Opt. 55, 10299 (2016).

The proposed method reconstruct the best phase image by minimizing a cost function (J) that counts the number of phase jumps

$$J = M \bullet N - \sum_{p=1}^{M}\sum_{q=1}^{N} \text{binarization}(\hat{\varphi})$$

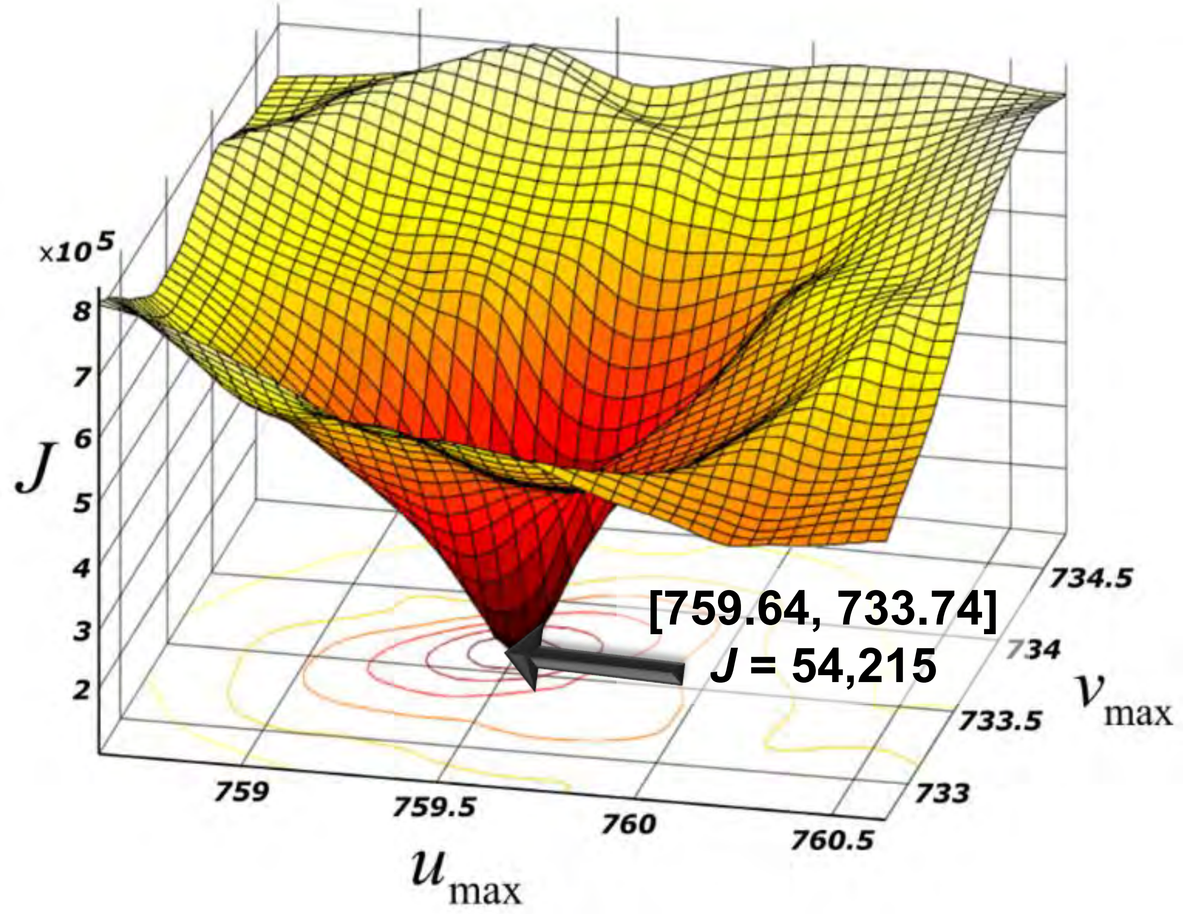

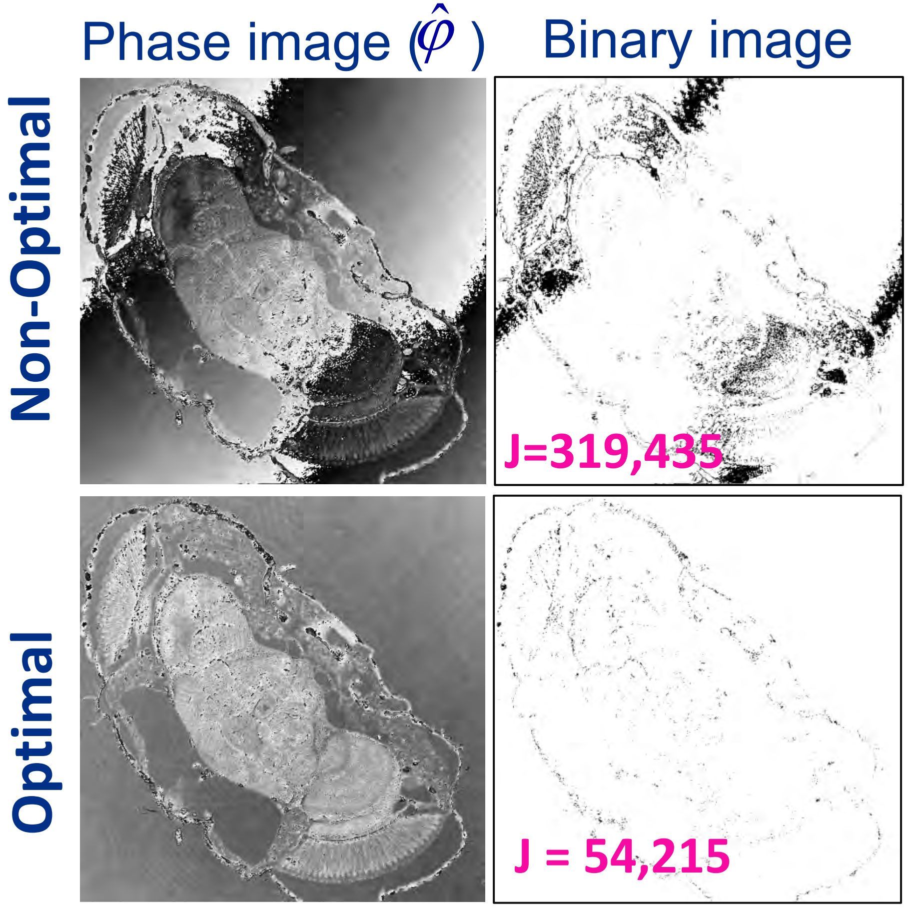

Castaneda & Doblas., Appl. Optics 60, 10214 (2021)

Fast & Accuracy Reconstruction QPI-DHM method

Sample	Phase USAF target			*Drosophila melanogaster* fly			Glioblastoma cells		
Method	NL	C	Our	NL	C	Our	NL	C	Our
Phase image					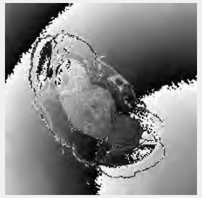		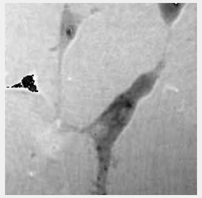		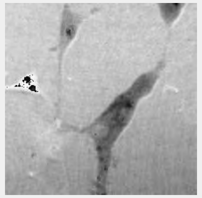
Image size	1024 × 1024			2048 × 2048			2048 × 2048		
u_{max}	149	149.85	149.27	760	761.08	759.64	512	512.08	512
v_{max}	297.2	296.46	296.13	734	735.65	733.74	357.2	357.28	357
Accuracy	0.88	0.93	0.95	0.82	0.80	0.97	0.98	0.81	0.99
Processing time (s)	60.2	3.8	1.6	236.7	7.3	3.3	238.2	7.7	2.6

https://github.com/oirl/tuDHM

NL = nested-for-loops method
C = centroid method

Castaneda & Doblas., Appl. Optics 60, 10214 (2021)

Unpredicted failing of tuDHM reconstruction method

Phase USAF target **Phase STAR target**

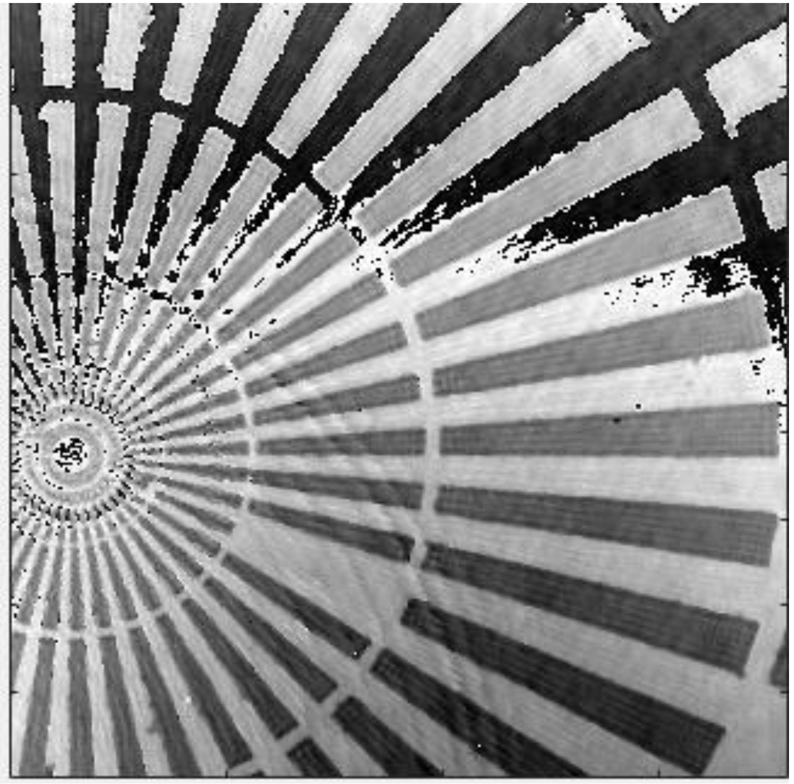

- ☒ Performance highly dependent on the sample.
- ☒ No recovery of phase maps at video rates

THE UNIVERSITY OF MEMPHIS

Learning-based reconstruction model to provide video-rate QPI-DHM

Recorded Hologram

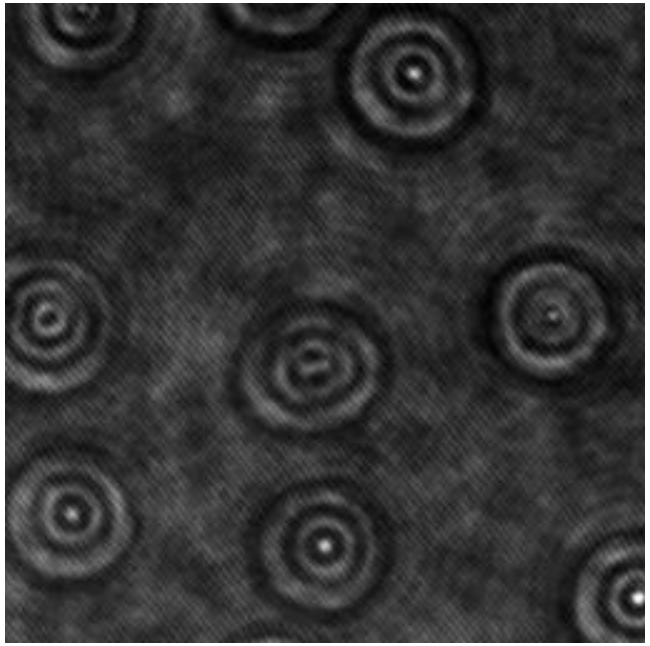

Deep Learning

Reconstructed Phase Image

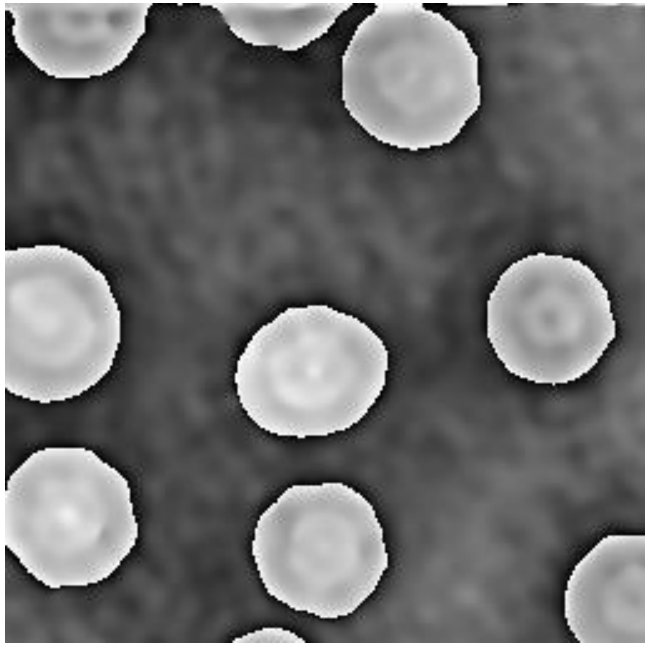

- ☑ Recovery of phase maps at video rates
- ☑ Performance should be independent of the sample with proper training

Castaneda & Doblas *et al.*, Proceeding IEEE (2021)
Castaneda & Doblas *et al.*, Sensors 21(23), 8021 (2021)

Experimental dataset for the learning-based model

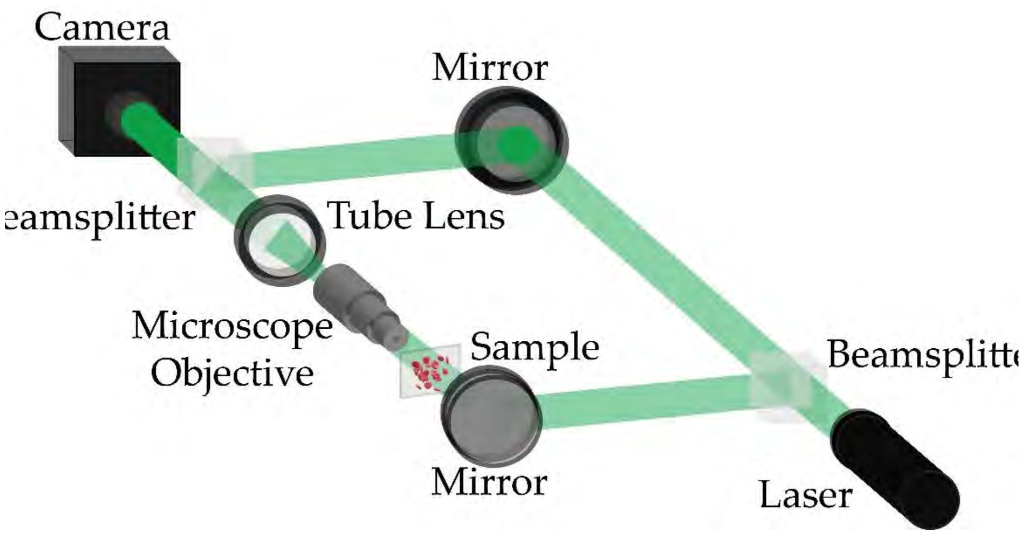

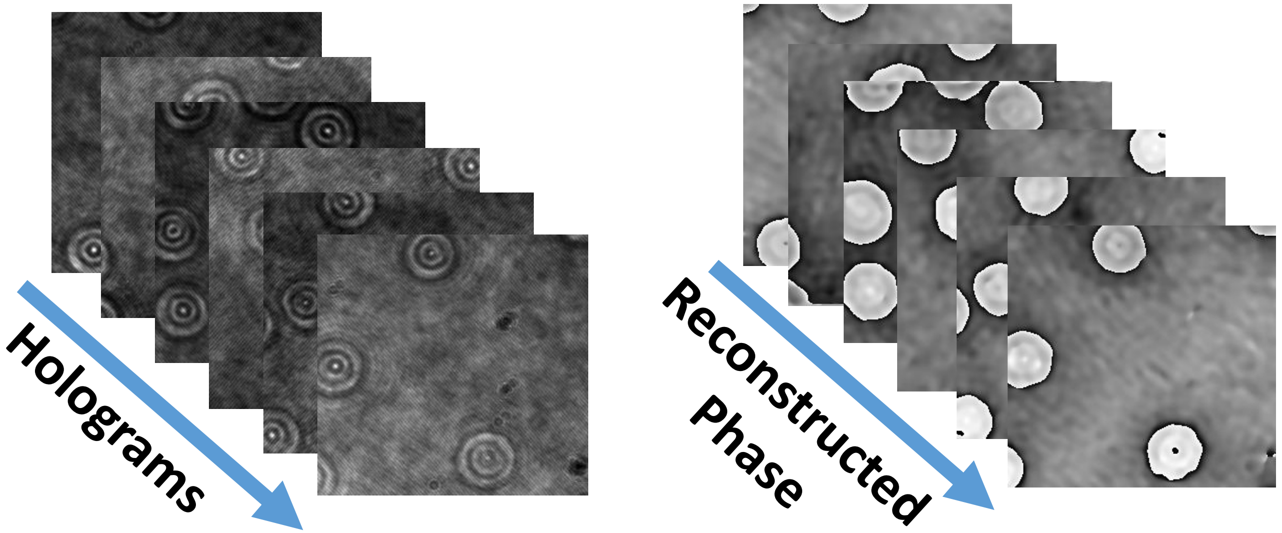

Details **MO:** 40×/0.65NA **CMOS:** 1920×1200 square pixels with side 5.86 μm

- ❑ Samples: unstained red blood cells (RBC).
- ❑ Dataset: recorded holograms (inputs) and aberration-free reconstructed phase images (output).
- ❑ Total number of images: 1,820 instances with images of 256x256 pixels.
- ❑ 80% and 20% of the dataset was used to train and validate the network, respectively.

THE UNIVERSITY OF MEMPHIS

Castaneda & Doblas ***et al.*****,** Sensors 21(23), 8021 (2021)

Conditional Generative Adversarial Network (cGAN)

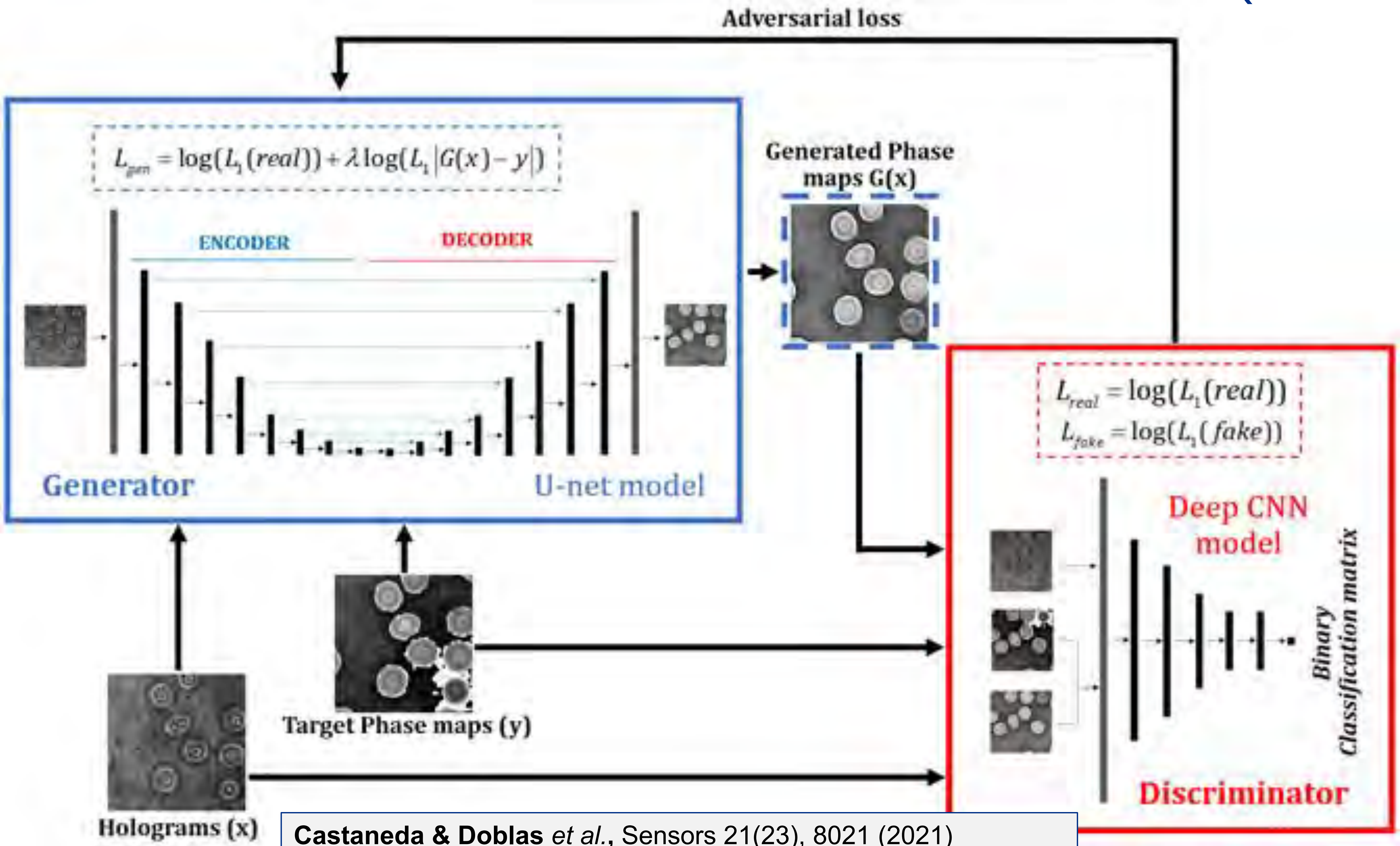

Castaneda & Doblas *et al.*, Sensors 21(23), 8021 (2021)

Innovation: inclusion of two customized metrics during training

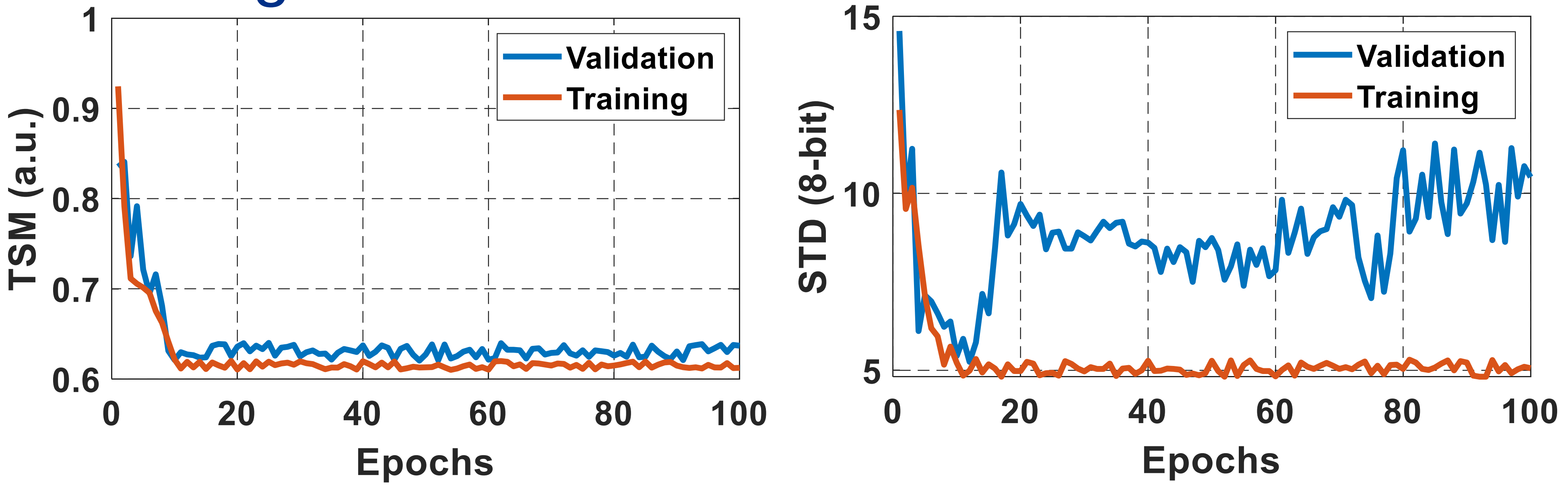

- ❑ TSM tracks the number of phase discontinuities using a thresholding-and-summation metric
- ❑ STD tracks the noise level measured in homogenous regions of the reconstructed phase maps using the standard deviation
- ☑ Our cGAN model has been trained using two customized metrics specifically designed for tracking the imaging characteristics in DHM.

THE UNIVERSITY OF MEMPHIS

Castaneda & Doblas ***et al.*****,** Sensors 21(23), 8021 (2021)

Rapid convergence in training thanks to the two customized metrics

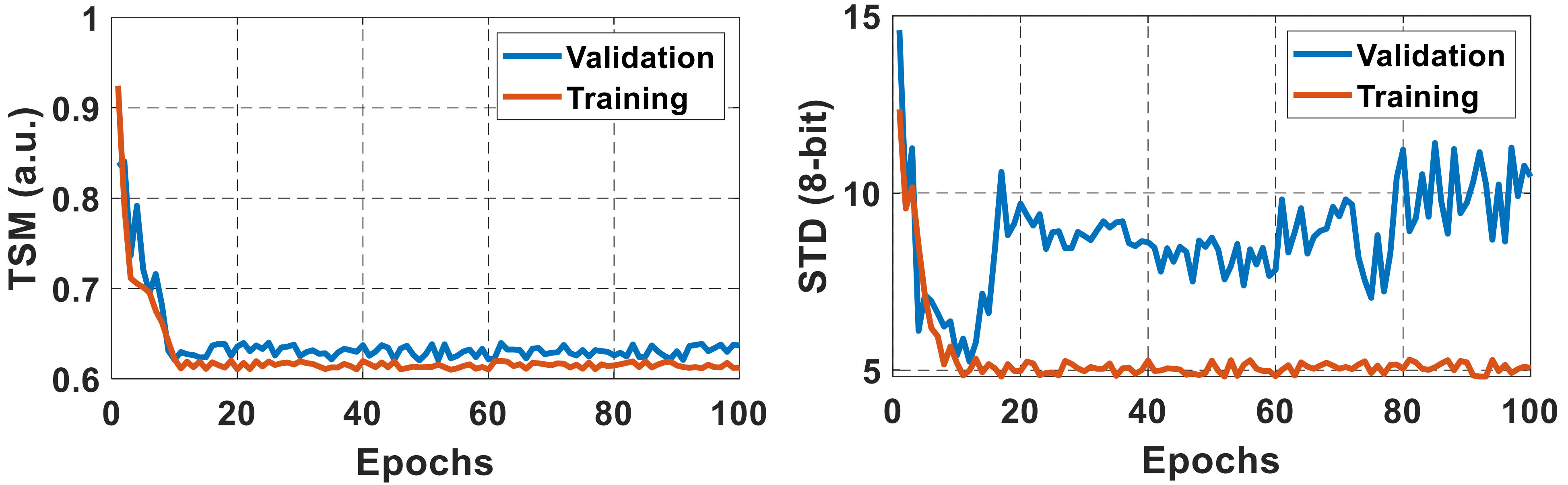

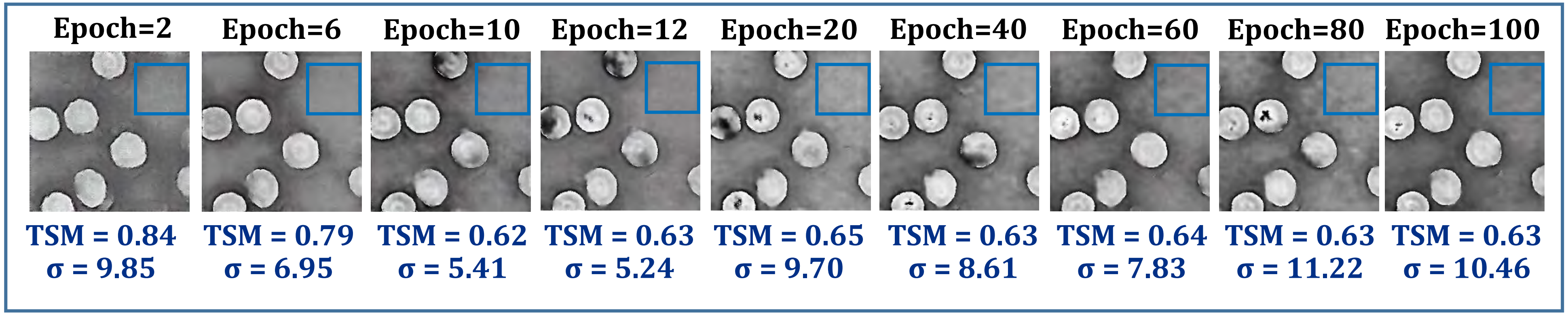

☑ TSM and STD metrics makes that the cGAN model converges rapidly (e.g., only 12 epochs are needed).

Castaneda & Doblas *et al.*, Sensors 21(23), 8021 (2021)

Validation of the cGAN model vs. the automatic method

- ❑The cGAN provides phase images free of phase distortions (e.g., reduced TSM values).
- ❑ The cGAN reduces speckle contrast (e.g., low STD values).

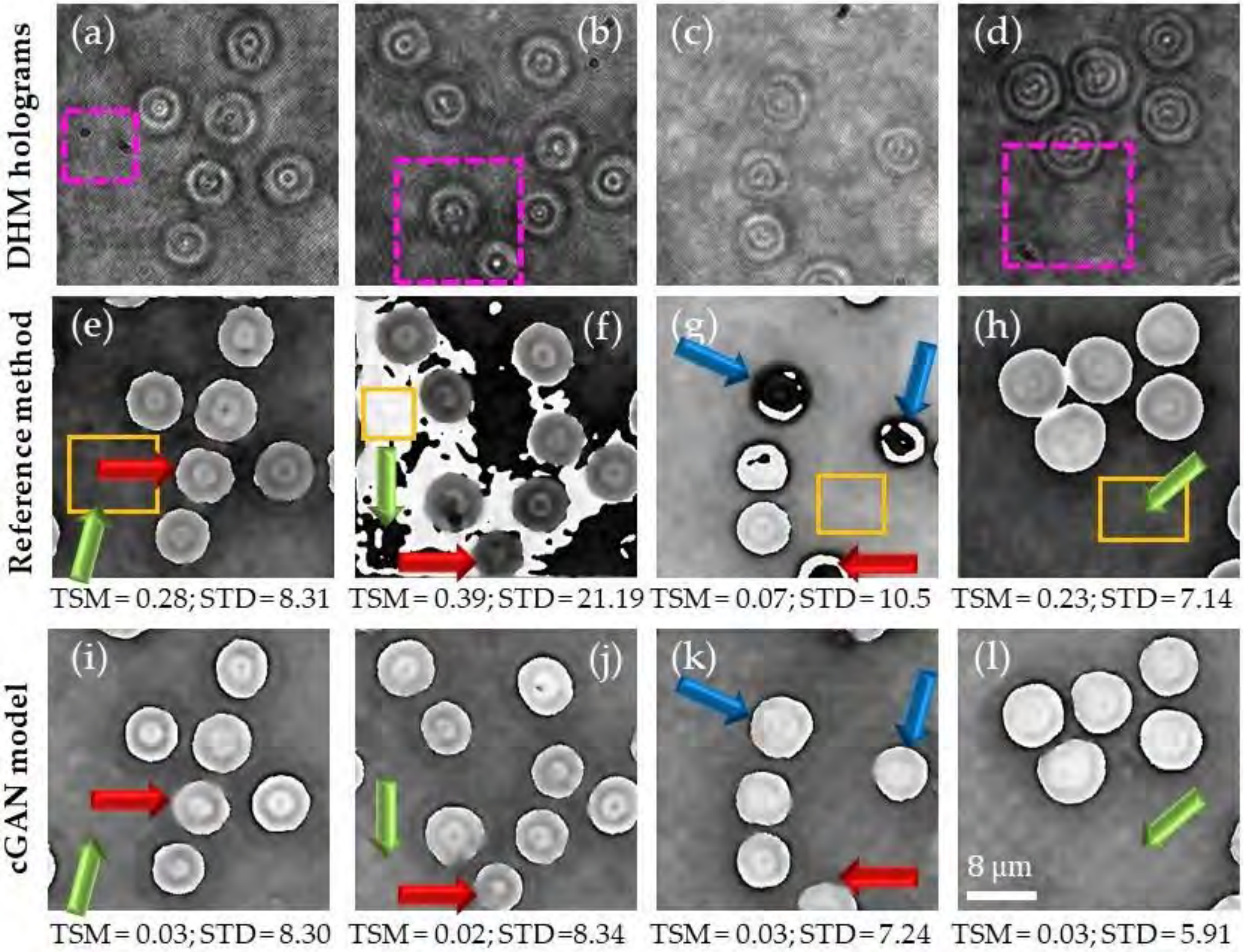

Castaneda & Doblas et al., Sensors 21(23), 8021 (2021)

Validation of the cGAN model to arbitrary holograms

- ❑Training dataset for U-Net was increased to 24,491.
- ❑The U-Net model provides distorted details of red blood cells.
- ❑The cGAN model reconstructs the
’

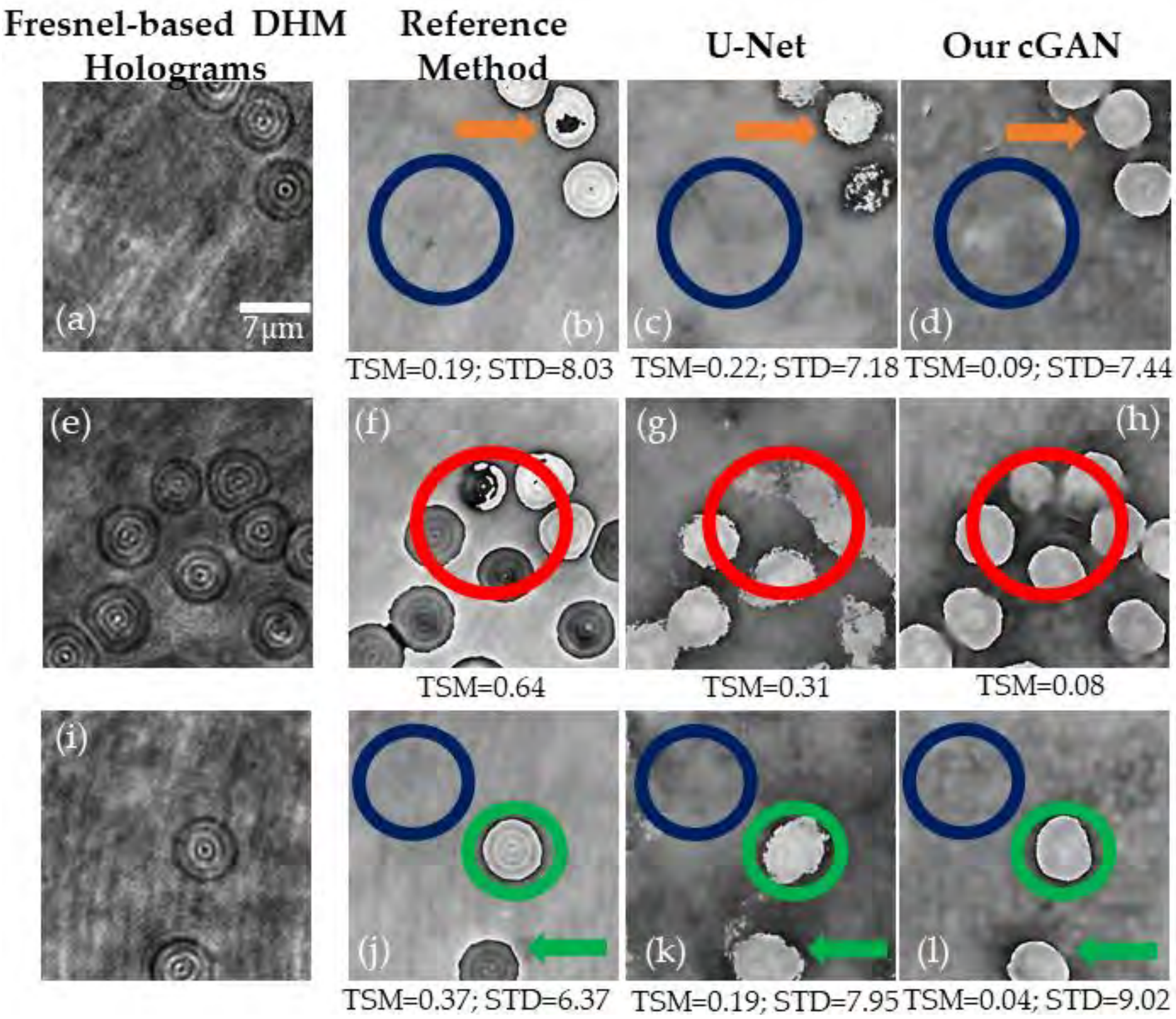

Castaneda & Doblas et al., Sensors 21(23), 8021 (2021)

OIRL Mission : Create open-source and automated tools for DHM

pyDHM Library:

- Utility Package
- Phase-Shifting Package
- Fully-Compensated Phase Reconstruction Package
- Numerical Propagation Package

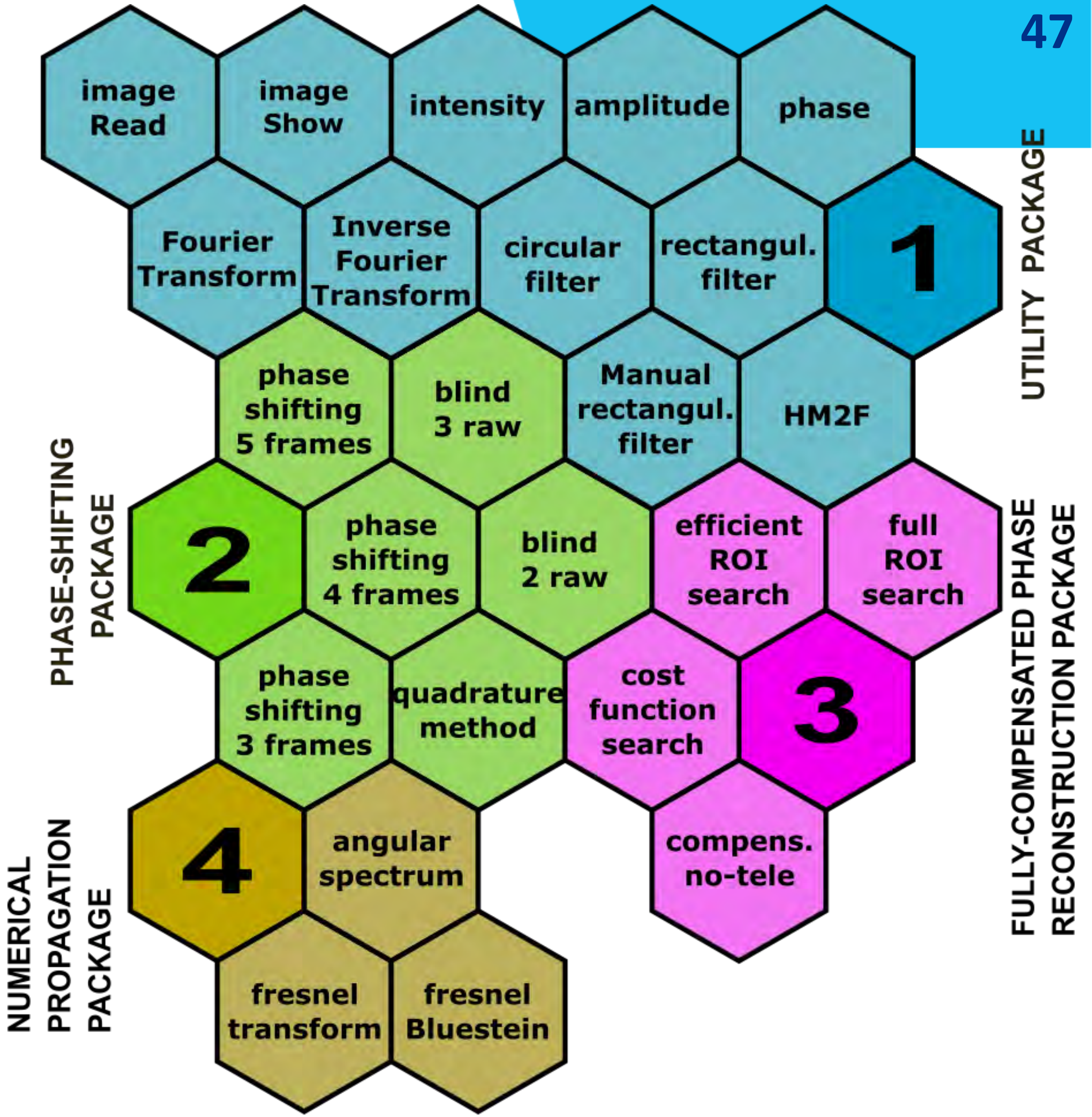

Castaneda & Doblas et al., PLOS ONE 17(10), e0275818 (2022).

Applications of lensless DHM to Marine Environment research

- **Monitoring of micro-organisms** in potable water, aiming to reduce water-related diseases[2]

- **Quantitative measurements for biodiversity and ecosystem monitoring[3]**: plankton concentration, average size and size dispersion of individuals, particle size dispersion, water turbidity, suspension statistics.

- **Potential** of real-time **plastic degradation** monitoring in a **marine** (saltwater) environment[4].

1

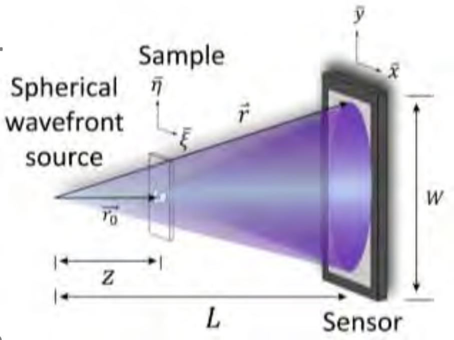

2

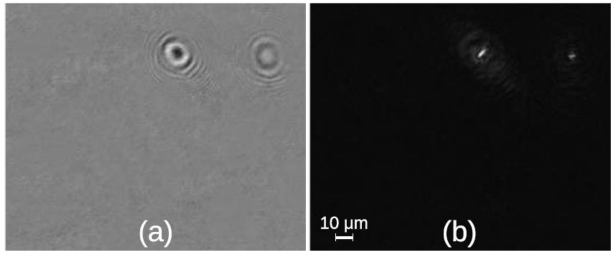

3

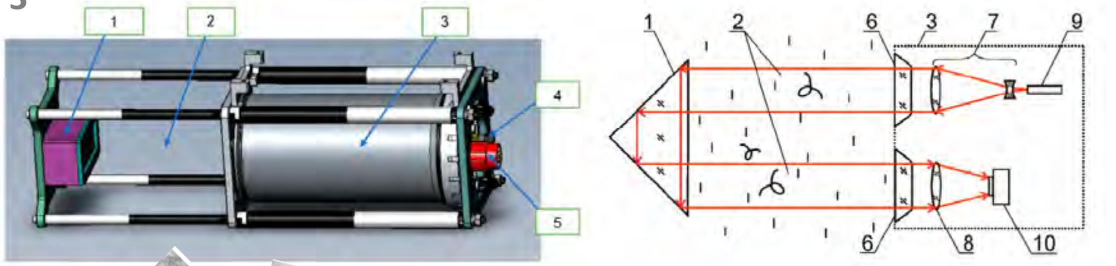

4

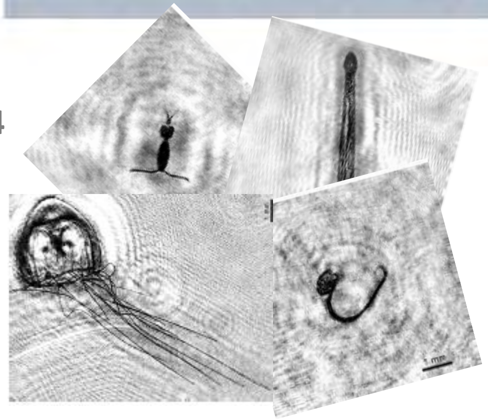

5

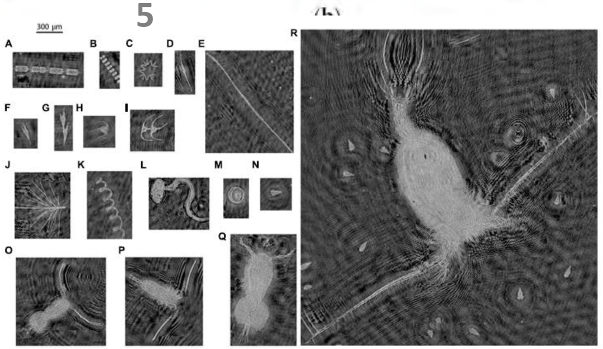

1. Credit to Maria Josef Lopera Acosta, Master dissertation, 2022.
2. Pitkaaho *et al.*, Digital Holography and 3D Imaging 2027, paper W2A.44 (2017)
3. Dyomin, *et. al.*, Sensors 21, 4863 (2021) & Dyomin *et al.*, Appl. Sci. 12, 11266 (2022) & Nayak *et al.*, Frontiers in Marine Science 7, 572146 (2021)
4. Schnitzler *et al.*, Marine Pollution Bulletin 163, 111950 (2021)).

Learning Objectives of this Research Seminar

- ❑ Differentiate between intensity-based and quantitative phase imaging techniques. ✓
- ❑ Learn the basics in hardware and computational method of off-axis DHM. ✓
- ❑ Recognize the advantages/disadvantages between telecentric and non-telecentric DHM systems ✓
- ❑ Understand the fundamentals of the common-path DHM. ✓
- ❑ Recognize the functioning reflection DHM systems for non-biological samples. ✓
- ❑ Realize the need for automated phase compensation algorithms to recover accurate information in off-axis DHM. ✓
- ❑ Recognize how learning-based models can be used in DHM. ✓

Acknowledgments

Collaborators

Dr. Carlos Trujillo, Department of Physical Sciences, EAFIT University, Medellin, Colombia
Dr. Bahram Javidi, Department of Electrical and Computer Engineering, University of Connecticut, CT.
Dr. Jorge Garcia-Sucerquia, School of Physics, Universidad Nacional de Colombia Sede Medellin, Colombia
Dr. Genaro Saavedra and Manuel Martinez-Corral, Department of Optics, Univ. of Valencia, Spain

Funding

This work has been funded in part by:
- The University of Memphis, Memphis, TN, USA
- National Science Foundation (2042563)

OIRL Research Group

Assistant Professor: Dr. A. Doblas (adoblas@memphis.edu)
Postdoctoral Researcher: Dr. R. Isaac (rohan.isaac@memphis.edu)
Graduate Students in OIRL Group: R. Castañeda, B. Bogue-Jimenez, S. Patra, K. Dahal
Undergraduate Students in OIRL Group: J. Brown, A. Abraham, and K. Balachandran

Watch our YouTube videos!
https://sites.google.com/view/oirl/workshop-in-digital-holographic-microscopy?authuser=0
https://sites.google.com/view/oirl/youtube

Optical Imaging Research Lab

Driven by doing. The University of Memphis